# Summer diatom blooms in the eastern North Pacific gyre investigated with a long-endurance autonomous surface vehicle

Emily E Anderson [1] , Cara Wilson [2] , Anthony H Knap [3] , Tracy A Villareal [Corresp. 1]

[1] Department of Marine Science and Marine Science Institute, The University of Texas at Austin, Port Aransas, Texas, United States of America

[2] National Marine Fisheries, National Oceanic and Atmospheric Administration, Monterey, California, United States of America

[3] Geochemical and Environmental Research Group, Texas A&M University, College Station, Texas, United States of America

Corresponding Author: Tracy A Villareal
Email address: tracyv@austin.utexas.edu

Satellite chlorophyll a (chl a) observations have repeatedly noted summertime phytoplankton blooms in the North Pacific subtropical gyre (NPSG), a region of open ocean that is far removed from any land-derived or Ekman upwelling nutrient sources. These blooms are dominated by $N_2$-fixing diatom-cyanobacteria associations of the diatom genera *Rhizosolenia* Brightwell and *Hemiaulus* Ehrenberg. Their nitrogen fixing endosymbiont, *Richelia intracellularis* J.A. Schmidt, is hypothesized to be critical to the development of blooms in this nitrogen limited region. However, due to the remote location and unpredictable duration of the summer blooms, prolonged *in situ* observations are rare outside of the Station ALOHA time-series off of Hawai'i. In summer, 2015, a proof-of–concept mission using the autonomous vehicle, *Honey Badger* (Wave Glider SV2), collected near-surface (<20m) observations in the NPSG using hydrographic, meteorological, optical, and imaging sensors designed to focus on phytoplankton abundance, distribution and physiology of this bloom-forming region. *Hemiaulus* and *Rhizosolenia* cell abundance was determined using digital holography for the entire June-November mission. *Honey Badger* was not able to reach the 30° N subtropical front region where most of the satellite chl a blooms have been observed, but near-real time navigational control allowed it to transect two blooms near 25° N. The two taxa did not co-occur in large numbers, rather the blooms were dominated by either *Hemiaulus* or *Rhizosolenia*. The 2-4 August 2015 bloom was comprised of 96% *Hemiaulus* and the second bloom, 15-17 August 2015, was dominated by *Rhizosolenia* (75%). The holograms also imaged undisturbed, fragile *Hemiaulus* aggregates throughout the sampled area at ~10 $L^{-1}$. Aggregated *Hemiaulus* represented the entire observed population at times and had a widespread distribution independent of the summer export pulse, a dominant annual event suggested to be mediated by aggregate fluxes. Aggregate occurrence was not

consistent with a density dependent formation mechanism and may represent a natural growth form in undisturbed conditions. The photosynthetic potential index ($F_v$:$F_m$) increased from ~0.4 to ~0.6 during both blooms indicating a robust, active phytoplankton community in the blooms. The diel pattern of $F_v$:$F_m$ (nocturnal maximum; diurnal minimum) was consistent with macronutrient limitation throughout the mission with no evidence of Fe-limitation despite the presence of nitrogen fixing diatom-diazotroph assemblages. During the 5-month mission, *Honey Badger* covered ~5690 km (3070 nautical miles), acquired 9336 holograms, and reliably transmitted data onshore in near real-time. Software issues developed with the active fluorescence sensor that terminated measurements in early September. Although images were still useful at the end of the mission, fouling of the LISST-Holo optics was considerable, and appeared to be the most significant issue facing deployments of this duration.

2 **Summer diatom blooms in the eastern North Pacific gyre investigated with a**

3 **long-endurance autonomous surface vehicle**

5 Emily E. Anderson[1],  Cara Wilson[2], Anthony H. Knap[3], Tracy A. Villareal[1]

7 [1] Department of Marine Science and Marine Science Institute, The University of Texas at Austin,

8 Port Aransas, Texas, United States of America

9 [2]
10 National Marine Fisheries, National Oceanic and Atmospheric Administration

11  Environmental Research Division, Monterey, California, United States of America

12 [33]Geochemical and Environmental Research Group, Texas A&M University, College Station,

13 Texas, United States of America

15 corresponding author:

16 Tracy Villareal[1]

17 Email address:  tracyv@austin.utexas.edu

**Abstract**

Satellite chlorophyll $a$ (chl $a$) observations have repeatedly observed summertime

phytoplankton blooms in the North Pacific subtropical gyre (NPSG), a region of open ocean that

is far removed from any land-derived or Ekman upwelling nutrient sources. These blooms are

dominated by $N_2$-fixing diatom-cyanobacteria associations of the diatom genera *Rhizosolenia*

Brightwell and *Hemiaulus* Ehrenberg.  Their nitrogen fixing endosymbiont, *Richelia*

*intracellularis* J.A. Schmidt,  is hypothesized to be critical to the development of blooms in this

nitrogen limited region. However, due to the remote location and unpredictable duration of the

summer blooms, prolonged *in situ* observations are rare outside of the Station ALOHA time-

series off of Hawai'i. In summer, 2015, a proof-of–concept mission using the autonomous

vehicle, *Honey Badger* (Wave Glider SV2), collected near-surface (<20m) observations in the

NPSG using hydrographic, meteorological, optical, and imaging sensors designed to focus on

phytoplankton abundance, distribution and physiology of this bloom-forming region. *Hemiaulus*

and *Rhizosolenia* cell abundance was determined using digital holography for the entire June-

November mission. *Honey Badger* was not able to reach the 30° N subtropical front region

where most of the satellite chl $a$ blooms have been observed, but near-real time navigational

control allowed it to transect two blooms near 25° N. The two taxa did not co-occur in large

numbers, rather the blooms were dominated by either *Hemiaulus* or *Rhizosolenia*. The 2-4

August 2015 bloom was comprised of 96% *Hemiaulus* and the second bloom, 15-17 August

2015, was dominated by *Rhizosolenia* (75%). The holograms also imaged undisturbed, fragile

*Hemiaulus* aggregates throughout the sampled area at ~10 L$^{-1}$. Aggregated *Hemiaulus*

represented the entire observed population at times and had a widespread distribution. The

distribution was independent of the summer export pulse, a dominant annual event suggested to

be mediated by  aggregate fluxes. Aggregate occurrence was not consistent with a density

45  dependent formation mechanism and may represent a natural growth form in undisturbed

46  conditions. The photosynthetic potential index ($F_v$:$F_m$) increased from ~0.4 to ~0.6 during both

47  blooms indicating a robust, active  phytoplankton community in the blooms. The diel pattern of

48  $F_v$:$F_m$ (nocturnal maximum; diurnal minimum) was consistent with macronutrient limitation

49  throughout the mission with no evidence of Fe-limitation despite the presence of nitrogen fixing

50  diatom-diazotroph assemblages. During the 5-month mission, *Honey Badger* covered ~5690 km

51  (3070 nautical miles), acquired 9336 holograms, and reliably transmitted data onshore in near

52  real-time. Software issues developed with the active fluorescence sensor that terminated

53  measurements in early September. Although images were still useful at the end of the mission,

54  fouling of the LISST-Holo optics was considerable, and appeared to be the most significant issue

55  facing deployments of this duration.

56

57

## Introduction

59       Low-nutrient, low chlorophyll (LNLC) oceanic regimes with chlorophyll $a$ (chl $a$)

60 concentrations $<0.07$ mg m$^{-3}$ constitute approximately 60% of the world ocean (Guieu et al.

61 2014) and are home to a phytoplankton community highly adapted for survival at the ambient

62 nanomolar concentrations of inorganic $NO_3^-$ and $PO_4^{-3}$. One of the important adaptations is

63 nitrogen-fixation (diazotrophy), a process by which dissolved $N_2$ is converted into ammonium

64 for incorporation into amino acids and proteins (Carpenter & Capone 2008). Dizaotrophy

65 requires abundant iron resources (Mills et al. 2004; Ratten et al. 2015) and is reduced in iron-

66 limited regions. $N_2$-fixation may also be limited by other nutrients (Kustka et al. 2002; Mills et

67 al. 2004; Ratten et al. 2015) or competition by non-diazotrophic phytoplankton (Weber &

68 Deutsch 2014). Multiple prokaryote taxa are capable of diazotrophy (Zehr & Kudela 2011);

69 photosynthetic taxa include colonial cyanobacteria such as *Trichodesmium* spp. (Capone et al.

70 1997; Goering et al. 1966), free-living coccoid forms including *Crocosphaera watsonii* (Goebel

71 et al. 2008; Zehr et al. 2001), and coccoid or filamentous forms symbiotic with eukaryotes. Of

72 these latter symbioses, there are coccoid forms symbiotic with the prymnesiophyte

73 *Braarudosphaera bigelowii* (Gran and Braarud) Deflandre (Thompson et al. 2014; Thompson et

74 al. 2012), dinoflagellates (Farnelid et al. 2010; Foster et al. 2006) and filamentous or coccoid

75 cyanobacteria occurring as exo- or endosymbionts of diatoms (Foster & O'Mullan 2008;

76 Villareal 1992). This latter group, diatom-diazotroph associations, are dominated by an

77 endosymbiosis between the filamentous cyanobacteria, *Richelia intracellularis*, and members of

78 the diatom genera *Rhizosolenia* and *Hemiaulus*. These symbioses have complex interactions with

79 their hosts (Foster & Zehr 2006; Hilton et al. 2013) and the taxonomic distinctness of the

80    symbionts even within a single host genus remains unclear. DDAs play important roles in

81    biogeochemical cycling off the Amazon (Carpenter et al. 1999; Subramaniam et al. 2008) and

82    Mekong Rivers (Bombar et al. 2011) as well as in the central North Pacific gyre (Church et al.

83    2008).

84          At the Hawai'i Ocean Time-series (HOT), episodic pulses of DDAs dominated by

85    *Hemiaulus* spp. rapidly sink to depth (Scharek et al. 1999a; Scharek et al. 1999b) and transport

86    ~20% of the annual benthic carbon flux in a limited window (15 July-15 August) termed the

87    (Karl et al. 2012). Isotopic signatures of $N_2$ fixation suggest that their diazotrophic symbiont is

88    present and fueling the biomass flux; the rapid sinking rate indicates aggregation plays a key role

89    in the accelerated transport to depth (Scharek et al. 1999b). The summer export pulse is possibly

90    linked to episodic surface blooms of DDAs advecting through the region in the prevailing flow

91    (Dore et al. 2008; Fong et al. 2008; White et al. 2007). Auxospore formation has also been

92    offered as an explanation (Karl et al. 2012) although direct examination of trap material (Scharek

93    et al. 1999a; Scharek et al. 1999b) reported no evidence of auxosporulation. Follett et al. (2018)

94    modelled generalized diatom-diazotroph association dynamics, noting that the population peaked

95    in the early summer and rapidly declined during the summer export pulse window after a

96    transition from modelled Fe to P limitation favored competitive exclusion by other taxa. The

97    model necessarily addressed generalized conditions and did not address the localized blooms

98    noted by satellites.  These blooms dominate in the summer (Wilson 2003) and are often

99    associated with the unique properties of mesoscale eddy flow-fields (Calil et al. 2011; Calil &

100   Richards 2010; Guidi et al. 2012). There are few long-term, high frequency direct observations

101   on diatom-diazotroph association abundance to evaluate these hypotheses.

102    In the N. Pacific, the diatom-diazotroph association host genus *Hemiaulus* is a

103    characteristic upper euphotic zone species typically found across the central North Pacific gyre at

104    concentrations of ~$10^2$ cells L$^{-1}$ (Venrick 1988; Venrick 1999). Near-surface blooms of both

105    *Rhizosolenia* and *Hemiaulus* DDAs at $10^4$+ cells L$^{-1}$ (Venrick 1974) extend well north of

106    Hawai'i at abundance up to $10^4$ L$^{-1}$ (Brzezinski et al. 1998; Krause et al. 2012; Villareal et al.

107    2011) and are frequently associated with summer chl *a* blooms observed in satellite ocean color

108    sensors (Villareal et al. 2011). These chl *a* blooms (operationally defined as > 0.15 mg chl *a* m$^{-3}$)

109    north of 25.5° N cover a much greater range of temperatures and surface area than the blooms at

110    HOT (~22.5° N) and extend at least as far north as 35.5° N (Villareal et al. 2012). While the data

111    suggest that these satellite-observed blooms are probably associated with diatom-diazotroph

112    association events, it has remained difficult to sample these more northerly blooms due to the

113    remote location, episodic timing and extensive geographic range. The applicability of the

114    summer export pulse to these areas is unclear, as is the general role of aggregation in *Hemiaulus*

115    spp. biology. *In situ* diver observations suggest aggregation commonly occurs in *Hemiaulus*

116    (Villareal et al. 2011), providing a means for rapid sinking as the bloom senesces. It is unclear

117    whether *Hemiaulus* aggregation occurs as a density dependent process as noted in coastal diatom

118    blooms (Burd & Jackson 2009; Jackson 2005), is a natural growth form of the genus similar to

119    *Rhizosolenia* mats, is uniquely localized to the summer export window, or is a more generalized

120    feature throughout the year. With recent observations of the ubiquitous presence of living diatom

121    cells in the 2,000-4,000 m depth strata, the role of aggregation in oceanic diatom biology has

122    assumed new importance (Agusti et al. 2015).

123     Sampling these blooms outside of HOT is a challenge due to both the distance to blooms,

124     unpredictable occurrence, long planning lead time, and cost involved in multiple week research

125     cruises. Even at HOT, shipboard sampling is at approximately monthly intervals and insufficient

126     to resolve episodic events in annual cycles. To address this, we used an SV2 Wave Glider

127     (*Honey Badger*), a long-range autonomous vehicle utilizing wave power for propulsion and solar

128     panel arrays on a surface float to provide power for a variety of sampling instruments (Daniel et

129     al. 2011). While many types of autonomous vehicles are used in the marine environment (Dickey

130     et al. 2008; Lee et al. 2017), the Wave Glider is particularly capable of multiple-month missions

131     carrying extensive payloads, is under near-real time control, and has successfully transited from

132     Hawai'i to Australia while returning oceanographic data (Villareal & Wilson 2014). They have

133     been successfully deployed for sediment transport studies (Van Lancker & Baeye 2015),

134     wind/current assessments of typhoons (Van Lancker & Baeye 2015), buoy validation exercises

135     (Fitzpatrick et al. 2015), examination of air-sea coupling in the Southern Ocean (Thomson &

136     Girton 2017), and processes controlling North Atlantic and Eastern Pacific Ocean salinity

137     variability (Lindstrom et al. 2017).

138     In our study, we equipped the Wave Glider *Honey Badger* with a novel array of imaging

139     and photophysiology sensors specifically targeting phytoplankton dynamics. We present data

140     gathered during a 5-month mission in 2015 which sampled two diatom blooms. The mission

141     objectives were to return the glider after 5 months with all sensors collecting useful data,

142     determine if a holographic imaging system could quantify diatom events, relate the abundance to

143     satellite observed chl *a* blooms, examine the data for *Hemiaulus* aggregations, and acquire

144     photosynthetic efficiency data using active fluorescence.

145

146 **Materials and Methods**

147       The mission area for the *Honey Badger* was the eastern North Pacific subtropical gyre

148 (NPSG) spanning 19-30° N and 144-157° W in the open waters northeast of the Hawaiian

149 Islands (Fig. 1) where chl *a* blooms regularly occur between July and October (Wilson 2003).

150 Waypoints were chosen based on Aqua-MODIS 8-day composite chl *a* concentration satellite

151 images from the Environmental Research Division's ERDDAP

152 (https://coastwatch.pfeg.noaa.gov/erddap/griddap/erdMBchla8day.html). After a preliminary

153 deployment in the test area off Kawaihae, Hawai'i, the *Honey Badger* headed north on 1 June

154 2015. It was recovered on 3 November 2015 and returned to the test facility for evaluation and

155 data download.

156       The Wave Glider® SV2 (Liquid Robotics, a Boeing company, Sunnyvale, CA) is an

157 autonomous surface vehicle capable of extended operations offshore. It has a surface float (2.1 m

158 x 0.6 m) connected by an umbilical (7 m in this application) to a subsurface glider (0.4 m x 1.9

159 m) with articulating wings (1.1 m wide) that uses vertical motion from waves to provide forward

160 movement. Within the surface float, equipment bays provide space for computers,

161 communications equipment and battery arrays powered by solar panels. Iridium satellite

162 communication with the Wave Glider *Honey Badger* used in this mission was in near-real time

163 and provided a near immediate ability to course correct and respond to environmental conditions.

164       The *Honey Badger* was equipped with sensors on the float, the sub-body, and on a towed

165 body (Fig. 2; Table 1) The float contained 2 Turner Designs C3 fluorometers (Sunnyvale, CA)

166 rimmed with anti-fouling copper, a Seabird Electronics gpCTD (Bellevue, WA) for water

167 temperature and salinity with an inline antifouling tablet, a Canon G10 camera (Canon, USA Inc,

168 Melville, NY) looking down through the float, a Datawell MOSE weather sensor (Datawell BV,

169 Haarlem, The Netherlands), Airmar WX and WS weather sensors+light bar (Airmar Technology

170    Corporation, Milford, NH), an AIS (automatic identification system) transponder and a radar

171    reflector. The sub-body located 7 m below the float had an externally mounted Turner Designs

172    PhytoFlash (Sunnyvale, CA) utilizing the data and power connections through the umbilical. The

173    PhytoFlash sensor was shielded by a dark cap painted inside and out with anti-fouling paint.  A

174    Sequoia Scientific, Inc. (Bellevue, WA) Laser *In Situ* Scattering and Transmissometry

175    Holographic System (LISST-Holo, termed Holo) was deployed in a neutrally buoyant towed

176    body behind the *Honey Badger* on a 10 m tether equipped with scoops to passively direct water

177    into the sample field. The tow fish varied from 6.3-15.5 m deep based on the Holo's internal

178    depth sensor. The Holo drew power from the umbilical with the data stored in the Holo's

179    onboard internal memory module. Bandwidth limitations did not permit transmission to shore via

180    Iridium satellite. The Holo sample chamber was painted with antifouling paint and lined with

181    copper tape on other surfaces to minimize fouling. Power consumption and available solar

182    charging dictated sampling frequency and varied with the sensors (Table 1). The vehicle reported

183    location and condition telemetry every 30 seconds. Sensors were integrated into the onboard

184    processing and communications equipment by Liquid Robotics with the exception of the

185    PhytoFlash. Software integration for the PhytoFlash and tow body construction was provided by

186    the Geophysical Engineering Research Group (GERG) at Texas A&M University.

187         The Turner C3 fluorometers were equipped with excitation and emission filters for chl *a*

188    a, phycoerythrin and colored dissolved organic material (CDOM) with values reported in

189    fluorescence units. The C3 sensors were deployed on either side of the centerline with a port and

190    starboard sensor. The port C3 sensor and optical port for the look-down camera were coated with

191    a ~30 μm layer of ClearSignal antifouling compound (Severn Marine Technologies, Annapolis,

192    MD) in spring, 2014. Due to technical difficulties, the mission was delayed a year with unknown

193   effects on the viability of the coating. The look-down camera began recording on 1 July 2015

194   and imaged vertically below the float for examining the umbilical and glider as needed but also

195   captured images of fish and biofouling over the course of the mission.

196         The Holo uses collimated laser light to create refraction patterns from particles that are

197   then recorded by camera to create a hologram (Davies et al. 2015). Software provided by

198   Sequoia Scientific Inc. (Holo_Batch v. 3.1) reconstructed multiple holograms into greyscale

199   images. Particle biovolume was calculated based on a cross-section area projected into a sphere.

200   Holo_Detail (v. 3.1) was used to process each hologram in greater detail to identify *Hemiaulus*

201   and *Rhizosolenia* spp. Isolated hologram areas could be imaged individually as 0.1-1 mm thick

202   sections allowing detailed images layer by layer. The sampling rate of 15 holographic images (30

203   s between images) every 6 hours was set prior to launch based on worst case power consumption

204   calculations and could not be modified once underway. The 15-image bursts taken every 6 hours

205   were combined to form one record yielding 4 records (bursts) $d^{-1}$. The Holo sampling volume

206   was 1.86 ml per image with the 15-image burst sampling a total of 27.9 ml. Dye studies prior to

207   the mission indicated the 30 second between images was sufficient for full chamber volume

208   replacement.

209         The large file size (~2 MB) of each raw Holo hologram precluded satellite transmission

210   and were only available for analysis after the *Honey Badger*'s recovery in November 2015. Upon

211   recovery of the drive, 9336 holographic images were analyzed with the Holo_Batch and

212   Holo_Detail at the University of Texas at Austin's Marine Science Institute. Comparison of

213   Holo_Batch processing and individual Holo_Detail processing of the same images indicated

214   progressive loss of recognizable diatoms over the mission due to biofouling (examples given in

215   Fig. S1). Therefore, *Hemiaulus* and *Rhizosolenia* cells were quantified using the Holo_Detail

216   software on every hologram with distinctive diffraction patterns indicating when particles were

217   present. While using the Holo_Detail to enumerate diatoms was more time-intensive than using

218   the montages of in-focus particles produced by the Holo_Batch, it was necessary as the montages

219   often failed to show *Hemiaulus* or *Rhizosolenia* cells when they were clearly identifiable in

220   Holo_Detail. The small size of individual *Hemiaulus* cells (~15 μm) and light silicification also

221   contributed to difficulties in using the batch analysis mode as biofouling interference increased.

222        The Holo's sampling capability allowed counting cells with a minimum concentration of

223   36 cells $L^{-1}$. Individual *Hemiaulus* cells were at the size threshold of the Holo and hard to

224   differentiate from other small cells unless they were in recognizable chains. In addition,

225   *Hemiaulus* cells occurred as both individual chains and aggregations of various size. Chains were

226   defined as 3 or more *Hemiaulus* cells which formed a curve with clear ends which did not cross

227   itself or others more than once. Aggregates were defined as *Hemiaulus* cells in a chain or

228   multiple chains with multiple ends or no discernable ends which crossed itself, other chains, or

229   other particles multiple times.

230        Hologram processing also returned calculated biovolume for all detected particles after

231   calculating their equivalent spherical diameter. The biovolume was automatically separated into

232   bins based on equivalent spherical diameter from 2.5 μm – 9, 847 μm (50 bins with the upper

233   size limit of each bin being 1.18 times the lower limit). The diatoms of interest in this study have

234   an equivalent spherical diameter between 13-60 μm so a subset of bins (13.1-58.1 μm) were

235   chosen to focus the analysis. Holograms with schlieren (optical anomalies in transparent

236   mediums), microbubbles or blank images were manually removed from the analyses.

237        Biofouling interference was removed using the manufacturer's recommended procedure

238   to average the biovolume over large groups of images. This procedure generated a constant

239    signal that represented a consistent particle presence assumed to be biofouling. We arbitrarily

240    averaged groups of 510 holograms representing an 8.5-day window for a total of 14 background

241    signatures. This signature was subtracted from each hologram in the specified window to

242    generate a biofouling-corrected biovolume. Details of this correction and effects on the result are

243    included as Supplemental Text and Fig. S1-S2.

244        Pulse Amplitude Modulation fluorometry (Schreiber 2004) determination of $F_v:F_m$

245    (PhytoFlash sample frequency=6 samples $hr^{-1}$) was used to evaluate phytoplankton

246    photophysiology. The PhytoFlash sampled at 10 minute intervals but was accelerated to 1 minute

247    intervals from 27-28 July to test the system's resiliency to increased sampling rates. The port C3

248    sensor was on a fixed 10 min sampling interval with 10 samples averaged to generate a single

249    value. The starboard sensor was reprogrammable via remote communications and was varied in

250    sampling timing and averaging at various points in the mission. Changes from multi-point

251    averaging to single point reporting resulted in systematic and predictable baseline shifts. The

252    reasons for these changes are unknown. Iron stress was evaluated using the variable fluorescence

253    criteria of Behrenfeld and Milligan (2013) simplified for the lower sampling rate of the

254    PhytoFlash.  In a macronutrient limited environment with sufficient iron, the nocturnal $F_v:F_m$ is

255    greater than the diurnal $F_v:F_m$. In an iron limited environment, the reverse is true. Time averaging

256    (nighttime average of 36 data points; 0800-1359 UTC and daytime average of 54 data points;

257    1800-0259 UTC) was required to obtain a stable signal and timed to avoid the observed

258    crepuscular $F_v:F_m$ excursions. The PhytoFlash shutdown and missed samples at an increasing

259    frequency during the mission and eventually failed completely in early September (traced to

260    software issues). To ensure a comparable day/night sampling, only periods with 75% or more of

261    the expected number of samples were included in the iron-limitation analysis and both periods

262      for a date were required to meet the above standard. These criteria resulted in the removal of 33

263      of the 94 days of data collected over the mission. The entire $F_v$:$F_m$ dataset was plotted versus

264      time for a visual inspection of the data as well.

265          Aqua MODIS satellite's 8-day composite of daily chl *a* was used to produce an animation

266      showing the development of the blooms in the NPSG during the 2015 bloom season (June-

267      November) and the position of the *Honey Badger*'s track (Video S1 at

268      https://figshare.com/articles/S1_movie_mp4/5993644). The raw data from the C3s, gpCTD, AIS,

269      MOSE, PhytoFlash, and weather station are archived at BCO-DMO (http://www.bco-

270      dmo.org/project/505589). The BCO-DMO site also contains the raw holograms, the biovolume

271      data, as well as the *Hemiaulus* and *Rhizosolenia* abundance data.

272

273      **Results**

274          Extensive biofouling on several of the optical windows occurred during the mission. A

275      time series of images from the look down camera illustrates the development over time of

276      barnacles and associated organisms (Fig. S3). A metal incompatibility with internal screw in the

277      LISST-Holo camera system mount resulted in significant corrosion (Fig. S4); however, it did not

278      encroach into the sample plane and no data was lost. *Honey Badger* collected 5 months of

279      salinity, surface water temperature, diatom abundance, photophysiology, and biovolume data

280      from the NPSG. A nine-point running average (Fig. 3, grey line) and daily average were used to

281      remove changes due to rain events or sensor errors in the gpCTD. The daily averaged water

282      salinity and temperature data (Fig. 3, color-coded by latitude) ranged from 22.8 to 27.8°C, and

283      34.6 to 35.6 salinity. The lower salinity water near Hawai'i is evident at the beginning and

284      ending of the mission. The *Honey Badger* did not cross the sub-tropical front, which is

285    characterized by salinity ~34.5 found at ~30° N (Wilson et al. 2013). The pronounced

286    temperature-salinity gradient from the center of the gyre to Hawai'i is evident in the continuous

287    decrease in salinity and increase in temperature along the straight line transect from the farthest

288    north point (29.245° N 152.40° W) on 12 Sept. 2015 to just north of Hawai'i on 23 Oct. 2015

289    (20.67° N 155.47° W).

290          The study area underwent a general chl *a* increase over the course of the mission that was

291    evident visually as a shift from deep blue to light green in mid-July ([Video S1](#)). This increase

292    was quantitatively expressed as the average of chl *a* values from all pixels in the study area (Fig.

293    4). Following a period of uniformly low chl *a* concentration throughout the study area in June-

294    July 2015 (Fig. 4), in mid-July chl *a* concentrations throughout the study area increased

295    concurrent with increased chl *a* variability (increased standard deviation around the mean) due to

296    chl *a* blooms ([Video S1](#)). This period of elevated bloom activity extended from 1 Aug to 15 Sept.

297    During this period, there were multiple blooms evident where the satellite chl *a* exceeded 0.2 mg

298    m$^{-3}$. The brief decrease in late September was followed by an increase in average chl *a* through

299    the end of the mission.

300          The two float-mounted Turner C3 fluorometers produced erratic signals and random

301    shifts in baseline values (Fig. 5). The sensors did not parallel each other except for a general

302    increase in the cyanobacteria pigment phycoerythrin from ~21 Sept. 2015 to the end of the

303    mission, nor did the satellite chl *a* values at *Honey Badgers* location note similar fluctuations.

304    The C3 data sets were excluded from further analysis due to a lack of an independent diagnostic

305    test to determine which data points were reflective of the water properties and which were noise

306    or errors introduced by the sensor.

307    *Hemiaulus* and *Rhizosolenia* cells were readily identifiable in the processed holograms

308    both as chains and aggregates (Fig. 6). *Hemiaulus* cells were identifiable as either curved or

309    spiral chains (Fig. 6a) as well as aggregates of varying degrees of complexity (Fig. 6b, c). With

310    three cells required to define identify a *Hemiaulus*, the minimum reported concentration is 108

311    cells $L^{-1}$. In *Rhizosolenia*, the symbiont of *Richelia intracelluaris* was visible as well (Fig. 6d

312    arrows). Mean *Hemiaulus* abundance over the entire mission was 303 cells $L^{-1}$ (s.d. = $1.0 \times 10^3$

313    cells $L^{-1}$, n = 610) and mean *Rhizosolenia* abundance was 63 cells $L^{-1}$ (s.d. = $2.7 \times 10^2$ cells $L^{-1}$,

314    n = 610) over all the samples. However, of the 610 samples, only 208 contained *Hemiaulus* cells

315    and 207 contained *Rhizosolenia* cells. When present, the average *Hemiaulus* abundance was 8.9

316    $\times 10^2 \, L^{-1}$ (s.d. = $1.6 \times 10^3$ cells $L^{-1}$, n = 208). Of the samples containing *Rhizosolenia* cells, the

317    average abundance was $1.8 \times 10^2$ cells $L^{-1}$ (s.d. = $4.5 \times 10^2$ cells $L^{-1}$, n = 207). *Hemiaulus*

318    maximum abundance in the averaged 15 image burst was $1.4 \times 10^4$ cells $L^{-1}$ on 2 August 2015

319    and the *Rhizosolenia* maximum abundance was $2.8 \times 10^3$ cells $L^{-1}$ on 16 August 2015 (Fig. 7).

320    Blooms were defined operationally as occurring when the abundance value was two s.d. above

321    the mean present values, resulting in a threshold of $4 \times 10^3$ cells $L^{-1}$ for *Hemiaulus* and $1 \times 10^3$

322    cells $L^{-1}$ for *Rhizosolenia.*

323    Surface chl *a* (satellite derived) at *Honey Badger's* position underwent a ~2 fold variation

324    over the mission (Fig. 7a) with a sharp increase on 2 Aug. 2015, followed by considerable day to

325    day patchiness evident throughout the rest of the mission. A similar pattern was seen in the

326    Phytoflash $F_m$ data from sub body at ~7 m (Fig. 7b) until the data collection failed on 1 Sept

327    2015. Two blooms were sampled, a *Hemiaulus* bloom on 2-4 August 2015 and a *Rhizosolenia*

328 bloom on 15-17 August 2015. Diatom abundance (Fig. 7c, d) was patchy with two order of

329 magnitude changes occurring within between adjacent Holo bursts in the blooms, a distance of

330 approximately 10 km. The *Hemiaulus* bloom was dominated by *Hemiaulus* (96% of total

331 diatoms; Fig. 7c) while the *Rhizosolenia* bloom was dominated by *Rhizosolenia* (75% of total

332 diatoms; Fig. 7d). However, neither bloom reached the 0.15 mg m$^{-3}$ chl *a* threshold used to

333 identify a satellite chl *a* bloom. The two blooms were separated in space and in time (Fig. 7, 8)

334 and both had increases in biovolume (Fig. 7e). The larger *Rhizosolenia* cells contributed nearly

335 2/3 more biovolume on 15-17 August 2015 despite the cell numbers being only 1/3 that of the

336 *Hemiaulus* bloom. The satellite chl *a* signature was still faint when *Honey Badger* sampled the

337 *Hemiaulus* bloom from 2-4 August 2015 (compare 8a and 8b) but continued to develop after the

338 *Honey Badger* left the area (Video S1). The *Rhizosolenia* bloom sampled by the *Honey Badger*

339 from 15-17 Aug 2015 did not have a well-defined satellite chl *a* signal (Fig. 7a,c; 8b). However,

340 the PhytoFlash F$_m$ (Fig. 7f) was approximately 33% higher in the *Rhizosolenia* bloom than the

341 *Hemiaulus* bloom.

342      Two declining blooms evident in the chl *a* animation were sampled (8/23-25/2015 and

343 9/14-16/2015; Video S1). In both cases, no aggregates were seen in the Holo and the maximum

344 local abundance ~300 cells L$^{-1}$ was reached in only one burst in each area. The rest of the bursts

345 were devoid of *Hemiaulus*. However, the lookdown camera imaged what appeared to be a mass

346 occurrence of small white flocs (Fig. S3b). Their identity could not be confirmed, but the size

347 and shape are consistent with either marine aggregates or possibly colonial radiolarians.

348      Maximum F$_v$:F$_m$ values (~0.6) were associated with the *Hemiaulus* and the *Rhizosolenia*

349 peak abundance values (Fig. 7e) although the data loss on 2 Aug. may have missed higher F$_v$:F$_m$

350    values. During the period of the two blooms (2-17 Aug), the $F_v$:$F_m$ values underwent day to day

351    changes in magnitude that were visibly distinct from the period before and after.

352         The Holo captured 31 *Hemiaulus* aggregates in 23 sampling bursts (Table 2 and 8c,d) out

353    of 610 total bursts over the mission (3.8%) or 11% of samples when any *Hemiaulus* were

354    present. Aggregates shared common characteristics of curled chains of various sizes tangled

355    together to create a characteristic shape (Fig. 6) and were easily identified when compared to

356    diver-collected aggregates (Fig. S5). When present, 72±25% (std. dev., n=23) of the total

357    *Hemiaulus* cells were present in aggregated form (Fig. 8c, Table 2). They were not limited to

358    regions where non-aggregated *Hemiaulus* cells were abundant (Fig. 8c, d) and were observed

359    from 27 June 2015 and 25 October 2015 with 13 of the 24 locations outside the time window of

360    the summer export pulse (green shading in 8d). Within the holograms containing *Hemiaulus*

361    aggregates, the average number of identifiable aggregated cells was 47±42 (std. dev, n = 31) with

362    a minimum of 7 (two small crossed chains) and a maximum of 220. Due to the complex 3-

363    dimensional structures of some of the aggregates, it is likely that cell counts for aggregates are

364    underestimates.

365         A single aggregate in a 15 image burst represents, on average, 36 aggregates $L^{-1}$.

366    Maximum abundance was present during the *Hemiaulus* bloom (2-4 Aug. 2015) where

367    normalized abundance was 108 aggregates $L^{-1}$. The highest sustained aggregate abundance was

368    during the early August bloom when aggregates were observed in 6 of 9 successive days (Table

369    2). However, there was no significant relationship between aggregated and non-aggregated cell

370    abundance ($r^2$=0.12, *p*=0.5, n=23) overall in the data set.  On 3 of the 23 bursts where aggregates

371    were observed, they were the only form of *Hemiaulus* present.

372    The $F_v$:$F_m$ values underwent diel excursions typical of high-light populations

373    experiencing solar-induced photoinhibition and down-regulation of photosynthetic activity where

374    yields were greatest in the dark period and lower during the daytime (Fig. 9a). Crepuscular

375    excursions were evident in many, but not all diel rhythms. From visual inspection of the entire

376    mission dataset, there was no reversal of the diel rhythm suggestive of Fe-stress. The quantitative

377    diurnal:nocturnal $F_v$:$F_m$ ratio remained positive indicative of a macro-nutrient limited

378    environment (Fig. 9b) although there was a long-term downward slope. The near zero values

379    after 1 September 2015 were the result of compromised PhytoFlash data as the $F_o$ and $F_m$ values

380    simultaneously drifted upwards resulting in loss of $F_v$:$F_m$ (details in Fig. S6). 31 Aug. 2015 was

381    the last date with uncompromised data before the PhytoFlash completely shutdown on 9

382    September 2015.

383

384    **Discussion**

385    **The Wave Glider SV2 as a sampling platform**

386    The Wave Glider SV2 *Honey Badger* successfully returned from a 5 month mission with

387    all sensors undamaged. All sensors reported data, although at varying frequency and reliability,

388    throughout the mission with the exception of the PhytoFlash. As a prototype mission, it was

389    successful at deploying and recovering optical and imaging sensors specific to phytoplankton

390    research questions. Individual sensors suffered from degradation associated with either platform

391    computer software issues (PhytoFlash) or environmental biofouling (C3s and the LISST-Holo).

392    Post-mission inspection by Turner Designs indicated the PhytoFlash operated properly

393    when removed from the glider, suggesting the system interface with the glider had failed. The

394    SV2 was the first production model of Wave Gliders. The customized software used to power

395    and communicate with the PhytoFlash was not part of the original system's dedicated software

396   and gradually created insurmountable conflicts that led eventually to a complete failure. The

397   newer generation (SV3) has a more robust on-board computer interface more amenable to

398   customization and this is not likely to be a future issue.

399       One of the goals of the mission was to sample regions with chl *a* concentrations >0.15

400   mg m$^{-3}$. The waypoints for glider were partially chosen based on the Aqua MODIS's chl *a* data.

401   Daily images were often incomplete due to cloud cover as well as being outside the daily

402   imaging path. The 8-day composite of the Aqua MODIS satellite data provided a more complete

403   image of the regional chl *a* concentrations, However, the 8 day images used for daily decision

404   making on the glider's movements were based on data that may have been up to 4 days old. This

405   delay resulted in a few missed sampling opportunities ([Video S1](#)) since chl *a* maps of the region

406   the data were incomplete as waypoints were determined. This was particularly evident in the

407   August *Hemiaulus* bloom. The magnitude of the bloom was not evident in the satellite imagery

408   until the glider was a week past it and nearly halfway to a developing bloom to the west.

409

410   **Biological observations**

411       During the June to November timeframe of this mission, *Hemiaulus* and *Rhizosolenia*

412   were the dominant diatom genera observed by the Holo in the NPSG  chl *a* blooms, reaffiming

413   Guillard and Kilham's (1977) characterization of these taxa as persistent diatom representatives

414   of the oligotrophic open ocean flora. The Holo's resolution limit (~15 μm) could not image the

415   smaller pennate diatoms such as *Mastogloia* that frequently co-dominate in these blooms. The

416   *Hemiaulus* abundance ($10^{4}$ cells L$^{-1}$) noted in the 2-4 August 2015 bloom is consistent with

417   previous reports of open Pacific Ocean blooms where *Mastogloia* is a co-dominant (Brzezinski

418    et al. 1998; Scharek et al. 1999a; Venrick 1974; Villareal et al. 2012). Thus, it is probable that

419    additional diatoms were present and contributing to the satellite chl *a* signature.

420        The patchiness in the abundance of *Hemiaulus* and the *Rhizosolenia* symbiosis was

421    unexpected. Approximately 2/3 of the bursts contained neither of these taxa. In some cases, the

422    next sampling burst (6 hours later, or approximately 10 km) would observe $\sim 10^3$-$10^4$ cells $L^{-1}$.

423    Such variation has been noted before from discrete ship sampling stations (Fong et al. 2008;

424    Venrick 1974; Villareal et al. 2012) but with little ability to sustain 6 hour sampling intervals for

425    months. The most extreme gradients were associated with developing blooms suggesting that the

426    factors driving blooms are highly localized and not represented by the average nutrient or

427    hydrographic characteristics. Calil (2011) reported satellite chl *a* features in this gyre developed

428    rapidly at frontal interfaces between mesoscale features as the result of sub-mesoscale

429    ageostrophic flows resulting in transient up and downwelling. This spatial development scale is

430    consistent with the abundance increase noted in the two observed diatom blooms and warrants

431    further investigation into the role that mesoscale frontal features play in diatom-diazotroph

432    association dynamics. However, there are no mechanisms suggested to address the variability in

433    the background concentrations ($10^1$-$10^2$ cell $L^{-1}$) of these taxa presumably adapted to uniformly

434    oligotrophic conditions.

435        Unlike previous studies using settled water samples or nets, we were able to record and

436    partition *Hemiaulus* into aggregated or unaggregated abundance. *Hemiaulus* aggregates

437    (Villareal et al. 2011) occurred throughout the mission, even in regions of low non-aggregated

438    *Hemiaulus* abundance (Fig. 7, 9). The presence of 1 or more aggregates usually dominated the

439    total abundance (Table 2) and on 3 occasions represented the entire *Hemiaulus* biomass seen.

440    Maximum abundance (108 aggregates $L^{-1}$) and  highest sustained aggregate abundance were both

441    present during the *Hemiaulus* bloom (2-4 Aug. 2015) where aggregated *Hemiaulus* represented

442    29-56% of the total *Hemiaulus* present in the bursts.

443       With an aggregate occurrence in 11% of the samples containing *Hemiaulus*, we examine

444    what principles of diatom aggregation are relevant in this environment. Jackson's general

445    coagulation model for diatom aggregates (Jackson 1990a; Jackson 1990b) suggest senescence,

446    elevated concentrations, and enhanced stickiness play a key role in aggregation formation. In our

447    data, aggregate density was highest in the August bloom, consistent with this model. However,

448    the long chains and elevated $F_v:F_m$ suggests a rapidly growing *Hemiaulus* population and the

449    continued increase in the bloom area chl *a* after *Honey Badger* departed (Video S1) suggests that

450    this bloom was sampled early in its development. The aggregated form dominated total

451    abundance when present, and aggregates appeared largely monospecific, at least within the

452    resolution limits of the Holo. In contrast, diatom aggregates in coastal waters scavenge other

453    particles and can sweep the water clear as they sink (Alldredge & Gotschalk 1989; Alldredge &

454    Gotschalk 1990; Alldredge & Silver 1988). We suggest that aggregated forms of *Hemiaulus* are

455    not solely the result of high rates of collision and sticking between *Hemiaulus* cell. Much like

456    *Rhizosolenia* mats (Villareal & Carpenter 1989), they may be a natural growth form of

457    *Hemiaulus* that results from curled chains twisting back on themselves. Further collisions may

458    play a role but appear unlikely in the low density conditions that generally prevailed in this

459    study.

460       Combined diver and net collections in 2003 (Villareal et al. 2011) found high *Hemiaulus*

461    abundance was coupled to an aggregation snowstorm (Fig. S5) and allows us to examine whether

462    the Holo's aggregate abundance data is credible. Using net-collected abundance data from the

463    2003 bloom (maximum abundance: 2,500 cells $L^{-3}$) and our average cells per aggregates in this

464 study (47), we calculate a potential for ~50 aggregates L$^{-1}$ for the 2003 *Hemiaulus* snowstorm.

465 The aggregates visible to divers (cm-sized) are substantially larger than the aggregates observed

466 by the Holo (mm-sized), so this is likely an overestimate of abundance in the 2003 snowstorm.

467 However, the value is similar to the detection limit represented by 1 aggregate per 15 image

468 Holo burst (36 aggregates L$^{-1}$) and suggests the Holo data are the correct order of magnitude.

469 Combined with the high proportion of samples containing aggregates (11%), our limited sample

470 volume (~28 ml), the broad aggregate distribution, and the lack of a satellite signature from the

471 2003 snowstorm (Villareal et al. 2011), we conclude that dense *Hemiaulus* aggregation events

472 are more common than reported. Pilskaln et al (2005) reported marine snow aggregates on the

473 order of 1-10 L$^{-1}$ at 28-30° N along a transect from HI to CA suggesting that *Hemiaulus*

474 aggregates are part of rich collection of macroscopic particles rarely sampled. The incidental

475 observation from the lookdown camera in a fading bloom of what appeared to be large

476 aggregates in a fading bloom were at too low a density to be sampled by the Holo, but

477 sufficiently large to be visible to the camera (Fig. S3b). Multiple imaging technologies on the

478 vehicle are clearly needed to further detail this type of event.

479      Regularly occurring *Hemiaulus* aggregates could be an important food source to

480 organisms in the open ocean due to their high concentration of carbon and nitrogen. They could

481 also play an important role in the global carbon cycle since aggregated forms, when

482 physiologically stressed, tend to sink much faster than non-aggregated particles (Stemmann &

483 Boss 2012) and can scavenge other suspended particles as they sink to depth (Alldredge & Silver

484 1988). Station ALOHA sediment trap data indicated that during the 13 year record, the  summer

485 export pulse resulted in ~ 20% of the annual carbon export to the benthos at >5,000 m (Karl et al.

486 2012) with high sinking rates ($10^2$ m d$^{-1}$) requiring aggregates as a dominant mode of transport

487  (Scharek et al. 1999a; Scharek et al. 1999b). Our data show that *Hemiaulus* aggregates extend

488  deep into the N. Pacific gyre and support the idea that the role of the summer export pulse may

489  be much wider than Sta. ALOHA waters near Hawai'i. However, there is no evidence that

490  aggregate formation, per se, is linked to the hypothesized annual rhythm driving the summer

491  export pulse. They occur independently of the summer export pulse.

492       We found no evidence of iron limitation during our sampling with the caveat that the

493  PhytoFlash measures a property of the phytoplankton community present, not a diatom-

494  diazotroph association specific stress. However, even during the *Hemiaulus* and *Rhizosolenia*

495  blooms observed on 3 August 2015 and 16 August 2015, the Fe index did not suggest iron

496  limitation or iron stress. From 1 June 2015 to 31 Aug. 2015, the dark-averaged $F_v$:$F_m$ stayed

497  above the light-averaged values, agreeing with the 2006 study by Behrenfeld et al. (2006) which

498  classified this area as having a type I regime with low macronutrients but sufficient iron supplies.

499

500  **Conclusions**

501       The *Honey Badger* offered a unique look into the remote oligotrophic North Pacific

502  subtropical gyre during its 5 month, 5,690 km mission. While some of the sensors failed during

503  the mission (PhytoFlash) or produced uninterpretable data (C3s), the mission was a success in

504  that other sensors (LISST-Holo) recorded novel data over an extensive period of time (5-months)

505  and wide geographic extent, and the glider returned intact. *The Honey Badger* and its sensors

506  allowed for a persistent presence in the NPSG during the late summer/early fall bloom season.

507       The long-term deployment of both imaging and photosynthetic efficiency sensors on a

508  mobile sampling platform provided novel information on the composition and physiology of

509  remote diatom blooms. The region showed no evidence of iron limitation despite the presence of

510  DDAs at $10^4$ concentrations. *Hemiaulus* aggregates were widespread and observed outside the

511  15 July – 15 August summer  export pulse (Karl et al. 2012) window suggesting that the

512  predictable timing of the summer export pulse cannot be uniquely attributed to a rhythm in

513  aggregate formation. If aggregates are consistent vectors for vertical transport at some stage, then

514  the potential for a basin-wide summer export pulse is enhanced. When present, *Hemiaulus*

515  aggregates are abundant ($>10 \text{ L}^{-1}$) and dominate the total *Hemiaulus* present.  Their general

516  characteristics are distinct from coastal diatom aggregates and more similar to *Rhizosolenia* mats

517  (Alldredge & Silver 1982; Carpenter et al. 1977; Villareal et al. 2014), suggesting *Hemiaulus*

518  aggregates are a natural growth form. Their broad and persistent occurrence suggests they do not

519  have consistently high sinking rates. The PhytoFlash and the Holo data are generally uncoupled

520  from the satellite chl *a* concentrations which illustrates the added value of *in situ* sampling to

521  understand the community structure and photophysiological characteristics of these blooms in

522  remote open ocean habitats.

523

524  **Acknowledgements**

525      We wish to thank Liquid Robotics, a Boeing company, for providing the glider time as

526  part of the PacX Challenge award and our project manager Danny Merritt for his contributions to

527  the mission success. We acknowledge John Walpert (GERG) for adapting some of equipment to

528  the SV2. In addition, the skilled field testing and support provided by Brad Woolhiser, Chuck

529  Shaver, Dustin Boettcher, and Vas Podorean at the LR test facility in Kawaihae, HI is gratefully

530  acknowledged. We wish to thank Bob Simons (SWFSC/ERD) for putting the *Honey Badger* data

531  on ERDDAP and Lynn DeWitt (SWFSC/ERD) for creating the project website

532  (http://oceanview.pfeg.noaa.gov/MAGI).

533

534

**References**

536  Agusti S, González-Gordillo JI, Vaqué D, Estrada M, Cerezo MI, Salazar G, Gasol JM, and
537        Duarte CM. 2015. Ubiquitous healthy diatoms in the deep sea confirm deep carbon
538        injection by the biological pump. *Nature Communications* 6:7608. 10.1038/ncomms8608
539  Alldredge AL, and Gotschalk CC. 1989. Direct observations of the mass flocculation of diatom
540        blooms: characteristics, settling velocities and formation of diatom aggregates. *Deep-Sea*
541        *Research* 36:159-171.
542  Alldredge AL, and Gotschalk CC. 1990. The relative contribution of marine snow of different
543        origins to biological processes in coastal waters.  10:41-58.
544  Alldredge AL, and Silver MW. 1982. Abundance and production rates of floating diatom mats
545        (*Rhizosolenia castracanei* and *Rhizosolenia imbricata* var. *shrubsolei*) in the eastern
546        Pacific Ocean. *Marine Biology (Berlin)* 66:83-88.
547  Alldredge AL, and Silver MW. 1988. Characteristics, dynamics and significance of marine
548        snow. *Progress in Oceanography* 20:41-82.
549  Behrenfeld M, Worthington K, Sherrell RM, Chavez FP, Strutton P, McPhaden M, and Shea
550        DM. 2006. Controls on tropical Pacific Ocean productivity revealed through nutrient
551        stress diagnostics. *Nature (London)* 442:1025-1028. DOI:10.1038
552  Behrenfeld MJ, and Milligan AJ. 2013. Photophysiological expressions of iron stress in
553        phytoplankton. In: Carlson CA, and Giovannoni SJ, eds. *Annual Review of Marine*
554        *Science, Vol 5*, 217-246.
555  Bombar D, Moisander PH, Dippner JW, Foster RA, Voss M, Karfeld B, and Zehr JP. 2011.
556        Distribution of diazotrophic microorganisms and nifH gene expression in the Mekong
557        River plume during intermonsoon. *Marine Ecology-Progress Series* 424:39-U55.
558        10.3354/meps08976
559  Brzezinski MA, Villareal TA, and Lipschultz F. 1998. Silica production and the contribution of
560        diatoms to new and primary production in the central North Pacific. *Marine Ecology*
561        *Progress Series* 167:89-101.
562  Burd AB, and Jackson GA. 2009. Particle Aggregation. *Annual Review of Marine Science* 1:65-
563        90. 10.1146/annurev.marine.010908.163904
564  Calil PHR, Doney SC, Yumimoto K, Eguchi K, and Takemura T. 2011. Episodic upwelling and
565        dust deposition as bloom triggers in low-nutrient, low-chlorophyll regions. *Journal of*
566        *Geophysical Research-Oceans* 116:doi: C06030 06010.01029/02010jc006704. C06030
567        10.1029/2010jc006704
568  Calil PHR, and Richards KJ. 2010. Transient upwelling hot spots in the oligotrophic North
569        Pacific. *Journal of Geophysical Research-Oceans* 115:DOI: 10.1029/2009jc005360.
570        C02003 10.1029/2009jc005360
571  Capone DG, Zehr JP, Paerl HW, Bergman B, and Carpenter EJ. 1997. Trichodesmium, a
572        globally significant marine cyanobacterium. *Science (Washington, DC)* 276:1221-1229.
573        10.1126/science.276.5316.1221
574  Carpenter EJ, and Capone DG. 2008. Nitrogen fixation in the marine environment. In: Capone
575        DG, Bronk DA, Mulholland MR, and Carpenter EJ, eds. *Nitrogen in the Marine*
576        *Environment*: Elsevier, 141-198.
577  Carpenter EJ, Harbison RG, Madin LP, Swanberg NR, Biggs DC, Hulburt EM, McAlister VL,
578        and McCarthy JJ. 1977. *Rhizosolenia*  Mats. *Limnology and Oceanography* 22:739-741.

579  Carpenter EJ, Montoya JP, Burns J, Mulholland MR, Subramaniam A, and Capone DG. 1999.
580      Extensive bloom of a N₂-fixing diatom/cyanobacterial association in the tropical Atlantic
581      Ocean. *Marine Ecology-Progress Series* 185:273-283.
582  Church MJ, Bjorkman KM, Karl DM, Saito MA, and Zehr JP. 2008. Regional distributions of
583      nitrogen-fixing bacteria in the Pacific Ocean. *Limnology and Oceanography* 53:63-77.
584  Daniel T, Manley J, and Trenaman N. 2011. The Wave Glider: enabling a new approach to
585      persistent ocean observation and research. *Ocean Dynamics* 61:1509-1520.
586      10.1007/s10236-011-0408-5
587  Davies EJ, Buscombe D, Graham GW, and Nimmo-Smith WAM. 2015. Evaluating
588      Unsupervised Methods to Size and Classify Suspended Particles Using Digital In-Line
589      Holography. *Journal of Atmospheric and Oceanic Technology* 32:1241-1256.
590      10.1175/jtech-d-14-00157.1
591  Dickey TD, Itsweire EC, Moline MA, and Perry MJ. 2008. Introduction to the Limnology and
592      Oceanography Special Issue on Autonomous and Lagrangian Platforms and Sensors
593      (ALPS). *Limnology and Oceanography* 53:2057-2061.
594      10.4319/lo.2008.53.5_part_2.2057
595  Dore JE, Letelier RM, Church MJ, Lukas R, and Karl DM. 2008. Summer phytoplankton blooms
596      in the oligotrophic North Pacific Subtropical Gyre: Historical perspective and recent
597      observations. *Progress in Oceanography* 76:2-38.
598  Farnelid H, Tarangkoon W, Hansen G, Hansen PJ, and Riemann L. 2010. Putative N₂-fixing
599      heterotrophic bacteria associated with dinoflagellate-cyanobacteria consortia in the low-
600      nitrogen Indian Ocean. *Aquatic Microbial Ecology* 61:105-117. 10.3354/ame01440
601  Fitzpatrick PJ, Lau Y, Moorhead R, Skarke A, Merritt D, Kreider K, Brown C, Canon R, Hine G,
602      Lampoudi T, and Leonardi AP. 2015. A Review of the 2014 Gulf of Mexico Wave Glider
603      (R) Field Program. *Marine Technology Society Journal* 49:64-71. 10.4031/mtsj.49.3.14
604  Follett CL, Dutkiewicz S, Karl DM, Inomura K, and Follows MJ. 2018. Seasonal resource
605      conditions favor a summertime increase in North Pacific diatom–diazotroph associations.
606      *The ISME Journal*. 10.1038/s41396-017-0012-x
607  Fong AA, Karl DM, Lukas R, Letelier RM, Zehr JP, and Church MJ. 2008. Nitrogen fixation in
608      an anticyclonic eddy in the oligotrophic North Pacific Ocean. *Isme Journal* 2:663-676.
609      10.1038/ismej.2008.22
610  Foster RA, Carpenter EJ, and Bergman B. 2006. Unicellular cyanobionts in open ocean
611      dinoflagellates, radiolarians, and tintinnids: Ultrastructural characterization and immuno-
612      localization of phycoerythrin and nitrogenase. *Journal of Phycology* 42:453-463.
613  Foster RA, and O'Mullan GD. 2008. Nitrogen-fixing and nitrifying symbioses in the marine
614      environment. In: Capone DG, Bronk DA, Mulholland MR, and Carpenter EJ, eds.
615      *Nitrogen in the Marine Environment, 2nd Edition*. San Diego: Elsevier, 1197-1218.
616  Foster RA, and Zehr JP. 2006. Characterization of diatom-cyanobacteria symbioses on the basis
617      of nifH, hetR and 16S rRNA sequences. *Environmental Microbiology* 8:1913-1925.
618      10.1111/j.1462-2920.2006.01068.x
619  Goebel NL, Edwards CA, Carter BJ, Achilles KM, and Zehr JP. 2008. Growth and carbon
620      content of three different-sized diazotrophic cyanobacteria observed in the subtropical
621      North Pacific. *Journal of Phycology* 44:1212-1220. 10.1111/j.1529-8817.2008.00581.x
622  Goering JJ, Dugdale RC, and Menzel DW. 1966. Estimates of in situ rates of nitrogen uptake by
623      *Trichodesmium* sp. in the tropical Atlantic Ocean. *Limnology and Oceanography* 11:614-
624      620.

625 Guidi L, Calil PHR, Duhamel S, Bjoerkman KM, Doney SC, Jackson GA, Li B, Church MJ,
626       Tozzi S, Kolber ZS, Richards KJ, Fong AA, Letelier RM, Gorsky G, Stemmann L, and
627       Karl DM. 2012. Does eddy-eddy interaction control surface phytoplankton distribution
628       and carbon export in the North Pacific Subtropical Gyre? *Journal of Geophysical*
629       *Research-Biogeosciences* 117. 10.1029/2012jg001984
630 Guieu C, Aumont O, Paytan A, Bopp L, Law CS, Mahowald N, Achterberg EP, Marañón E,
631       Salihoglu B, Crise A, Wagener T, Herut B, Desboeufs K, Kanakidou M, Olgun N, Peters
632       F, Pulido-Villena E, Tovar-Sanchez A, and Völker C. 2014. The significance of the
633       episodic nature of atmospheric deposition to Low Nutrient Low Chlorophyll regions.
634       *Global Biogeochemical Cycles* 28:1179-1198. 10.1002/2014GB004852
635 Guillard RRL, and Kilham P. 1977. The ecology of marine planktonic diatoms. In: Werner D,
636       ed. *The Biology of Diatoms*. Berkeley: University of California Press, 372-346.
637 Hilton JA, Rachel AF, Tripp HJ, Brandon JC, Jonathan PZ, and Villareal TA. 2013. Genomic
638       deletions disrupt nitrogen metabolism pathways of a cyanobacterial diatom symbiont.
639       *Nature Communications* 4:1767-1767. 10.1038/ncomms2748
640 Jackson GA. 1990a. Limitation of algal blooms by formation of flocs through physical
641       coagulation. *EOS* 71:185.
642 Jackson GA. 1990b. A model of the formation of marine algal flocs by physical coagulation
643       processes. *Deep-Sea Research* 37:1197-1211.
644 Jackson GA. 2005. *Coagulation theory and models of oceanic plankton aggregation*. Boca
645       Raton: Crc Press-Taylor & Francis Group.
646 Karl DM, Church MJ, Dore JE, Letelier RM, and Mahaffey C. 2012. Predictable and efficient
647       carbon sequestration in the North Pacific Ocean supported by symbiotic nitrogen fixation.
648       *Proceedings of the National Academy of Sciences* 109:1842-1849.
649 Krause JW, Brzezinski MA, Villareal TA, and Wilson C. 2012. Increased kinetic efficiency for
650       silicic acid uptake as a driver of summer diatom blooms in the North Pacific gyre.
651       *Limnology and  Oceanography* 57:1084-1098. DOI: 10.4319/lo.2012.57.4.1084
652 Kustka A, Carpenter EJ, and Sanudo-Wilhelmy SA. 2002. Iron and marine nitrogen fixation:
653       progress and future directions. *Research in Microbiology* 153:255-262.
654 Lee CM, Paluszkiewicz T, Rudnick DL, Omand MM, and Todd RE. 2017. Autonomous
655       instruments significantly expand ocean observing An introduction to the special issue on
656       autonomous and lagrangian platforms and sensors (ALPS). *Oceanography* 30:15-17.
657       10.5670/oceanog.2017.211
658 Lindstrom EJ, Shcherbina AY, Rainville L, Farrar JT, Centurioni LR, Dong SF, D'Asaro EA,
659       Eriksen C, Fratantoni DM, Hodges BA, Hormann V, Kessler WS, Lee CM, Riser SC, St
660       Laurent L, and Volkov DL. 2017. Autonomous multi-platform observations during the
661       salinity processes in the upper-ocean regional study. *Oceanography* 30:38-48.
662       10.5670/oceanog.2017.218
663 Mills MM, Ridame C, Davey M, La Roche J, and Geider RJ. 2004. Iron and phosphorus co-limit
664       nitrogen fixation in the eastern tropical North Atlantic. *Nature (London)* 429:292-294.
665 Pilskaln CH, Villareal TA, Dennett M, Darkangelo-Wood C, and Meadows G. 2005. High
666       concentrations of marine snow and diatom algal mats in the North Pacific Subtropical
667       Gyre: Implications for carbon and nitrogen cycles in the oligotrophic ocean. *Deep-Sea*
668       *Research Part I-Oceanographic Research Papers* 52:2315-2332.
669 Ratten JM, LaRoche J, Desai DK, Shelley RU, Landing WM, Boyle E, Cutter GA, and Langlois
670       RJ. 2015. Sources of iron and phosphate affect the distribution of diazotrophs in the

671    North Atlantic. *Deep-Sea Research Part Ii-Topical Studies in Oceanography* 116:332-
672    341. 10.1016/j.dsr2.2014.11.012
673  Scharek R, Latasa M, Karl DM, and Bidigare RR. 1999a. Temporal variations in diatom
674    abundance and downward vertical flux in the oligotrophic North Pacific gyre. *Deep-Sea
675    Research Part I-Oceanographic Research Papers* 46:1051-1075.
676  Scharek R, Tupas LM, and Karl DM. 1999b. Diatom fluxes to the deep sea in the oligotrophic
677    North Pacific gyre at Station ALOHA. *Marine Ecology-Progress Series* 182:55-67.
678  Schreiber U. 2004. *Pulse-amplitude-modulation (PAM) fluorometry and saturation pulse
679    method: An overview*.
680  Stemmann L, and Boss E. 2012. Plankton and particle size and packaging: from determining
681    optical properties to driving the biological pump. In: Carlson CA, and Giovannoni SJ,
682    eds. *Annual Review of Marine Science, Vol 4*, 263-290.
683  Subramaniam A, Yager PL, Carpenter EJ, Mahaffey C, Bjorkman K, Cooley S, Kustka AB,
684    Montoya JP, Sanudo-Wilhelmy SA, Shipe R, and Capone DG. 2008. Amazon River
685    enhances diazotrophy and carbon sequestration in the tropical North Atlantic Ocean.
686    *Proceedings of the National Academy of Sciences of the United States of America*
687    105:10460-10465. 10.1073/pnas.0710279105
688  Thompson A, Carter BJ, Turk-Kubo K, Malfatti F, Azam F, and Zehr JP. 2014. Genetic diversity
689    of the unicellular nitrogen-fixing cyanobacteria UCYN-A and its prymnesiophyte host.
690    *Environmental Microbiology* 16:3238-3249. 10.1111/1462-2920.12490
691  Thompson AW, Foster RA, Krupke A, Carter BJ, Musat N, Vaulot D, Kuypers MMM, and Zehr
692    JP. 2012. Unicellular cyanobacterium symbiotic with a single-celled eukaryotic alga.
693    *Science (Washington, DC)* 337:1546-1550. 10.1126/science.1222700
694  Thomson J, and Girton J. 2017. Sustained Measurements of Southern Ocean Air-Sea Coupling
695    from a Wave Glider Autonomous Surface Vehicle. *Oceanography* 30:104-109.
696    10.5670/oceanog.2017.228
697  Van Lancker V, and Baeye M. 2015. Wave glider monitoring of sediment transport and dredge
698    plumes in a shallow marine sandbank environment. *PLoS ONE* 10:e0128948.
699  Venrick EL. 1974. The distribution and significance of *Richelia intracellularis* Schmidt in the
700    North Pacific Central Gyre. *Limnology and Oceanography* 19:437-445.
701  Venrick EL. 1988. The vertical distributions of chlorophyll and phytoplankton species in the
702    North Pacific central environment. *Journal of Plankton Research* 10:987-998.
703  Venrick EL. 1999. Phytoplankton species structure in the central North Pacific, 1973-1996:
704    variability and persistence. *Journal of Plankton Research* 21:1029-1042.
705  Villareal TA. 1992. Marine nitrogen-fixing diatom-cyanobacterial symbioses. In: Carpenter EJ,
706    Capone DG, and Reuter J, eds. *Marine Pelagic Cyanobacteria: Trichodesmium and other
707    Diazotrophs*. Netherlands: Kluwer, 163-175.
708  Villareal TA, Adornato L, Wilson C, and Shoenbachler CA. 2011. Summer blooms of diatom-
709    diazotroph assemblages (DDAs) and surface chlorophyll in the N. Pacific gyre – a
710    disconnect. *Journal of Geophysical Research-Oceans* 116:DOI: 10.1029/2010JC006268.
711    10.1029/2010JC006268
712  Villareal TA, Brown CG, Brzezinski MA, Krause JW, and Wilson C. 2012. Summer diatom
713    blooms in the North Pacific subtropical gyre: 2008-2009. *PLoS ONE* 7:e33109.
714    doi:33110.31371/journal.pone.0033109.

715 Villareal TA, and Carpenter EJ. 1989. Nitrogen-fixation, suspension characteristics and chemical
716     composition of *Rhizosolenia* mats in the central North Pacific Gyre. *Biological*
717     *Oceanography* 6:327-345.
718 Villareal TA, Pilskaln CH, Montoya JP, and Dennett M. 2014. Upward nitrate transport by
719     phytoplankton in oceanic waters: balancing nutrient budgets in oligotrophic seas. *PeerJ*
720     2:e302. 10.7717/peerj.302
721 Villareal TA, and Wilson C. 2014. A comparison of the Pac-X Trans-Pacific Wave glider data
722     and satellite data (MODIS, Aquarius, TRMM and VIIRS). *PLoS ONE* 9:e92280.
723     10.1371/journal.pone.0092280
724 Weber T, and Deutsch C. 2014. Local versus basin-scale limitation of marine nitrogen fixation.
725     *Proceedings of the National Academy of Sciences* 111:8741-8746.
726     10.1073/pnas.1317193111
727 White AE, Spitz YH, and Letelier RM. 2007. What factors are driving summer phytoplankton
728     blooms in the North Pacific Subtropical Gyre? *Journal of Geophysical Research-Oceans*
729     112. C12006 10.1029/2007jc004129
730 Wilson C. 2003. Late Summer chlorophyll blooms in the oligotrophic North Pacific Subtropical
731     Gyre. *Geophysical Research Letters* 30:1942, doi:1910.1029/2003GL017770.
732 Wilson C, Villareal TA, Brzezinski MA, Krause JW, and Shcherbina AY. 2013. Chlorophyll
733     bloom development and the subtropical front in the North Pacific. *Journal of*
734     *Geophysical Research: Oceans* 118:1-16. 10.1002/jgrc.20143
735 Zehr JP, and Kudela RM. 2011. Nitrogen Cycle of the Open Ocean: From Genes to Ecosystems.
736     In: Carlson CA, and Giovannoni SJ, eds. *Annual Review of Marine Science, Vol 3*, 197-
737     225.
738 Zehr JP, Waterbury JB, Turner PJ, Montoya JP, Omoregie E, Steward GF, Hansen A, and Karl
739     DM. 2001. Unicellular cyanobacteria fix $N_2$ in the subtropical North Pacific Ocean.
740     *Nature (London)* 412:635-638. 10.1038/35088063
741

# Figure 1

Mission track of the SV2 Wave Glider *Honey Badger*.

Mid-day positions points are color-coded by month. The asterisk north of Oahu is Station ALOHA of the Hawai'i Ocean Time-Series (HOT).
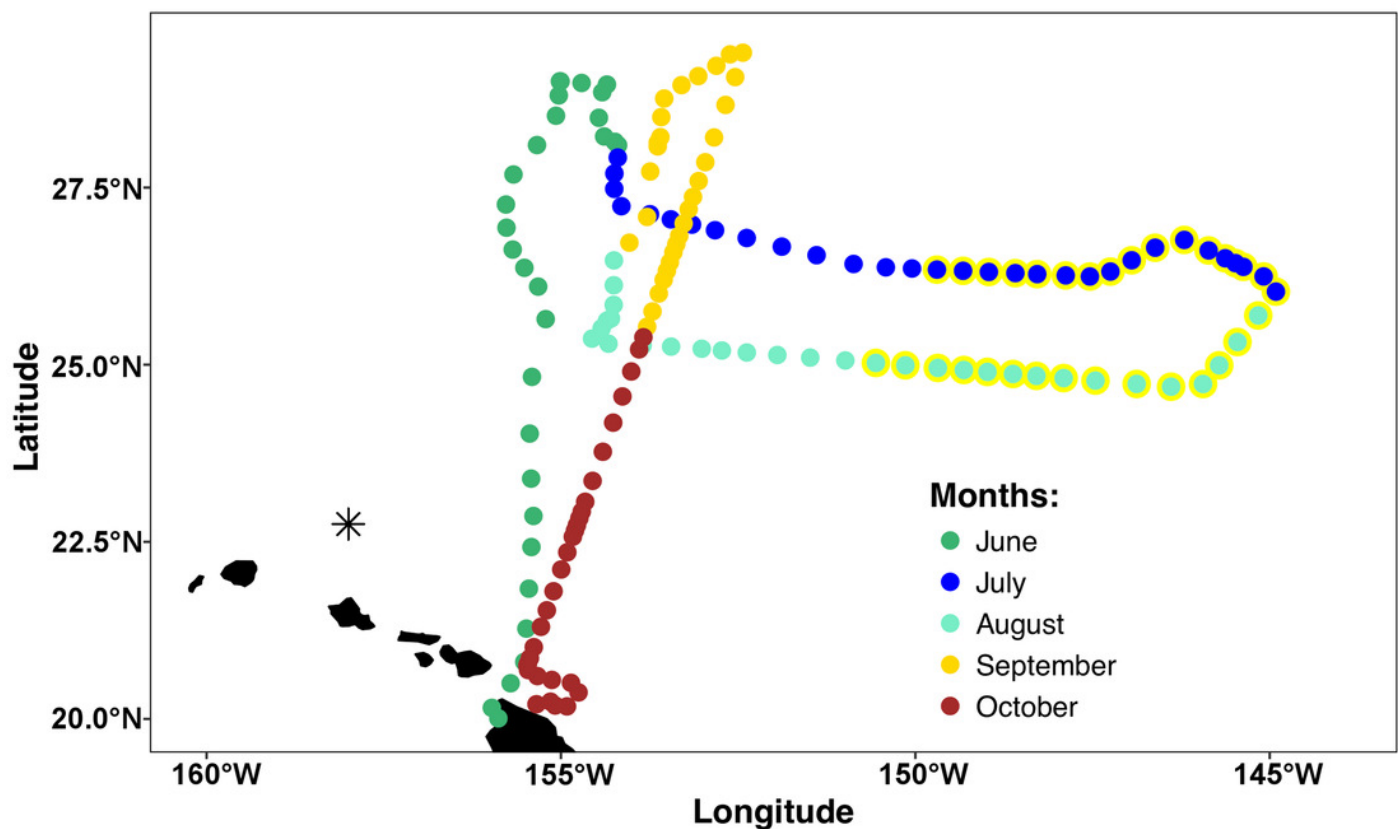
# Figure 2

*Honey Badger* diagram and sensor locations.

Schematic provided courtesy of Liquid Robotics, a Boeing Company.
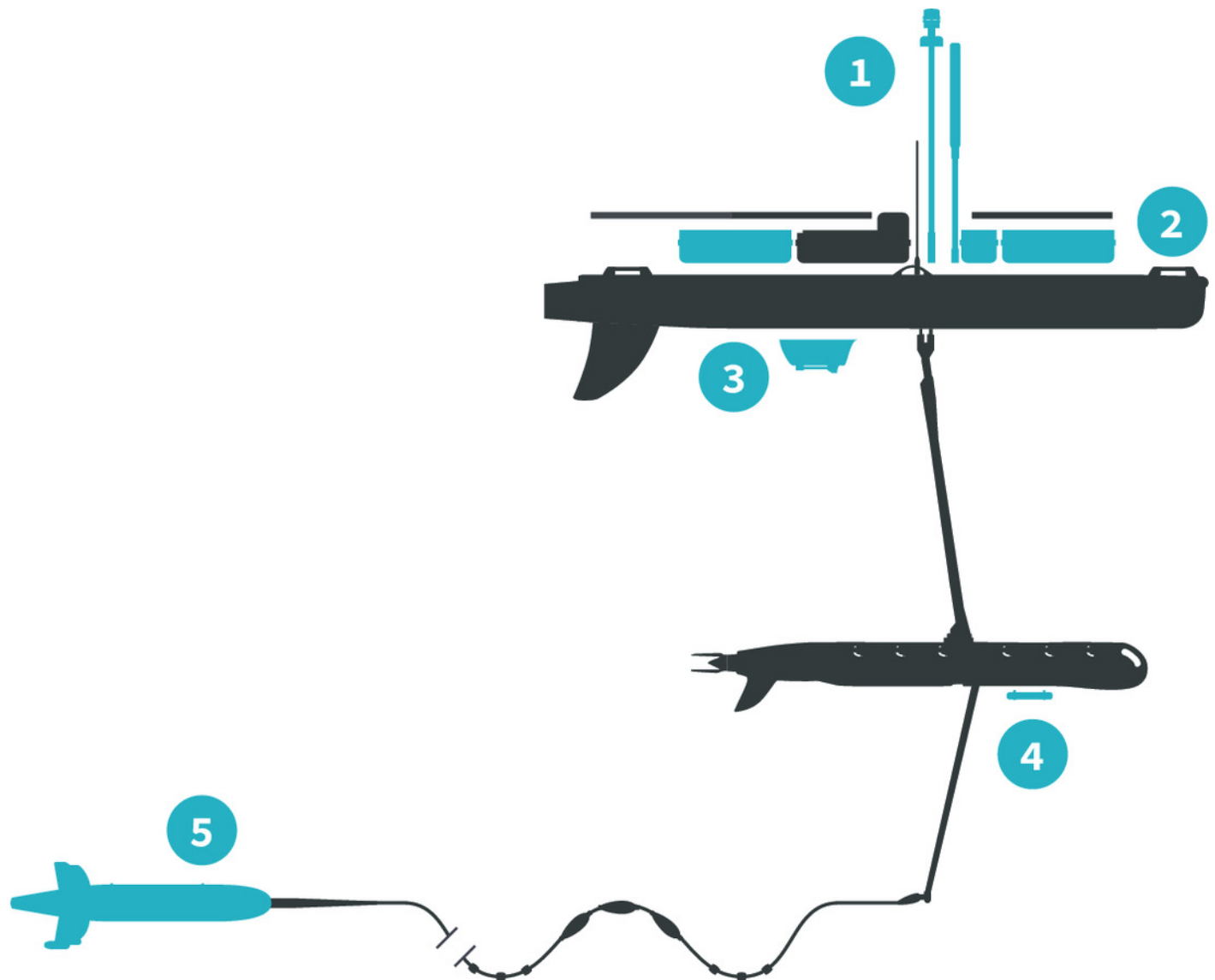
# Figure 3

Time series of the hydrographic properties from the *Honey Badger*'s gpCTD sensor.

(A) Salinity. (B) Temperature (°C). The grey lines are the data with a 9-point smoothing, the color-coded dots are daily average values.
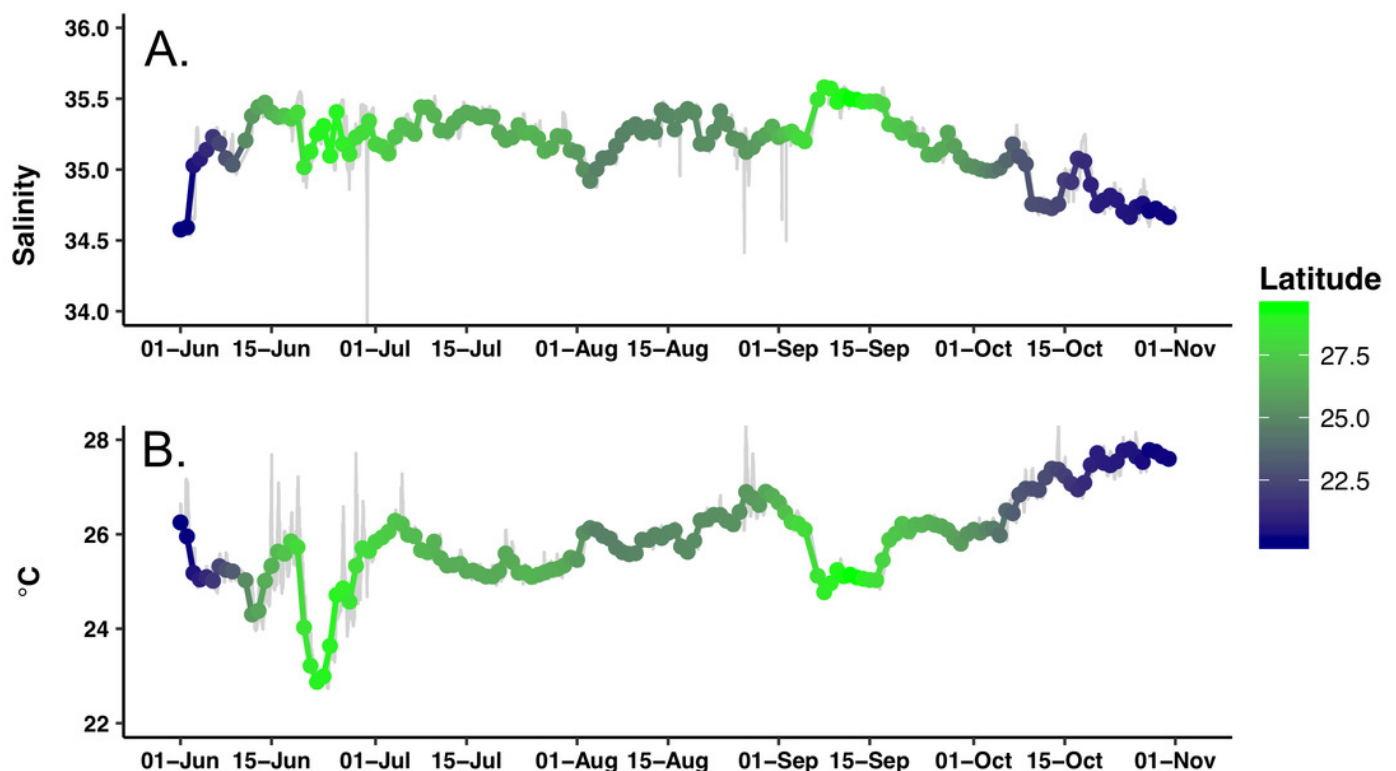
# Figure 4

Average chl *a* concentration of the study area over time.

All chl *a* per pixel values from Aqua MODIS 8-day composite data within the study area (bounded by 19 to 30°N and 157-144°W) were averaged to generate a single daily value for the study area. Solid line = average chl concentration for the study area. Dashed lines = average chl concentration ± 1 standard deviation.v
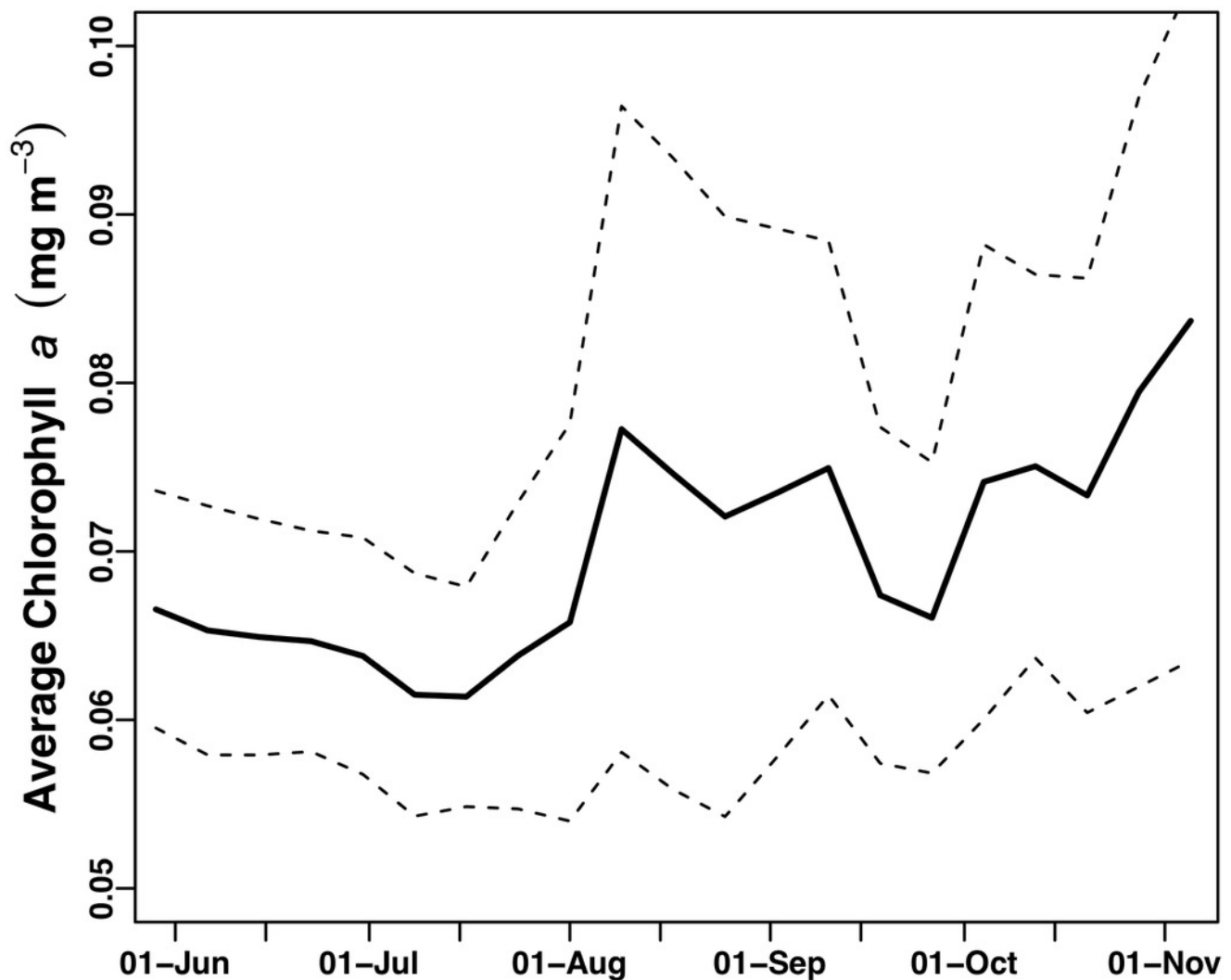
# Figure 5

C3 fluorometer data from the *Honey Badger*.

Note scale shifts between plots. (A-C) Sensor coated with antifouling compound. (A) Chl. (B) CDOM. (C) Phycoerythrin. (D-F) uncoated sensor. (D) Chl. (E) CDOM. (F) Phycoerythrin. RFU = relative fluorescence units.
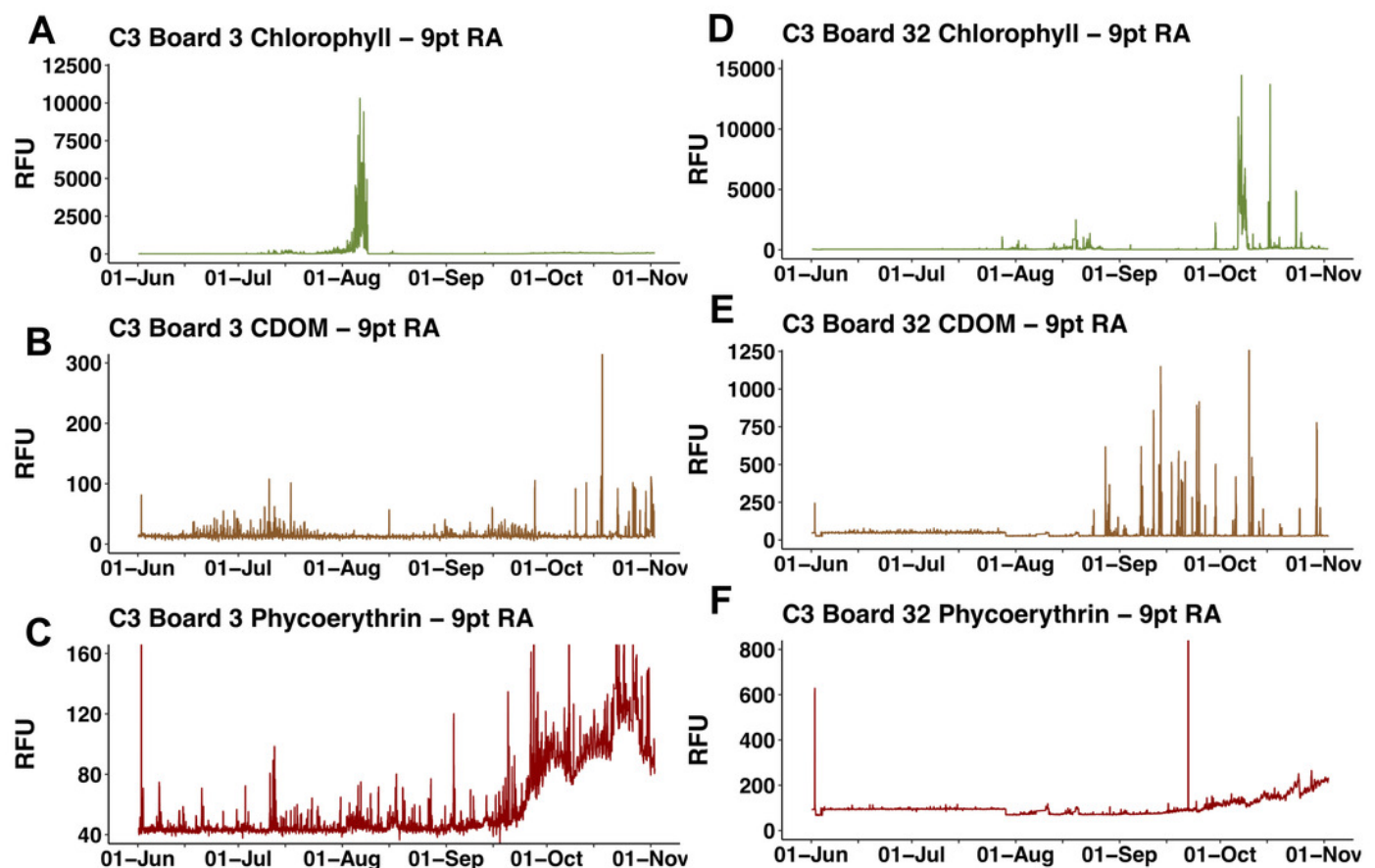
# Figure 6

Processed holographic images of *Hemiaulus* and *Rhizosolenia* cells and aggregates.

(A) Curved chain of *Hemiaulus hauckii*. Each dark dot is the cell mass separated from adjacent cells by siliceous structures. Images have been contrast enhanced for clarity. (B) *Hemiaulus* aggregate. (C) *Hemiaulus* aggregate. (D) Two complete *Rhizosolenia* cells and half of the next cell with their symbionts *Richelia* (arrows) located at the apex of the cells.
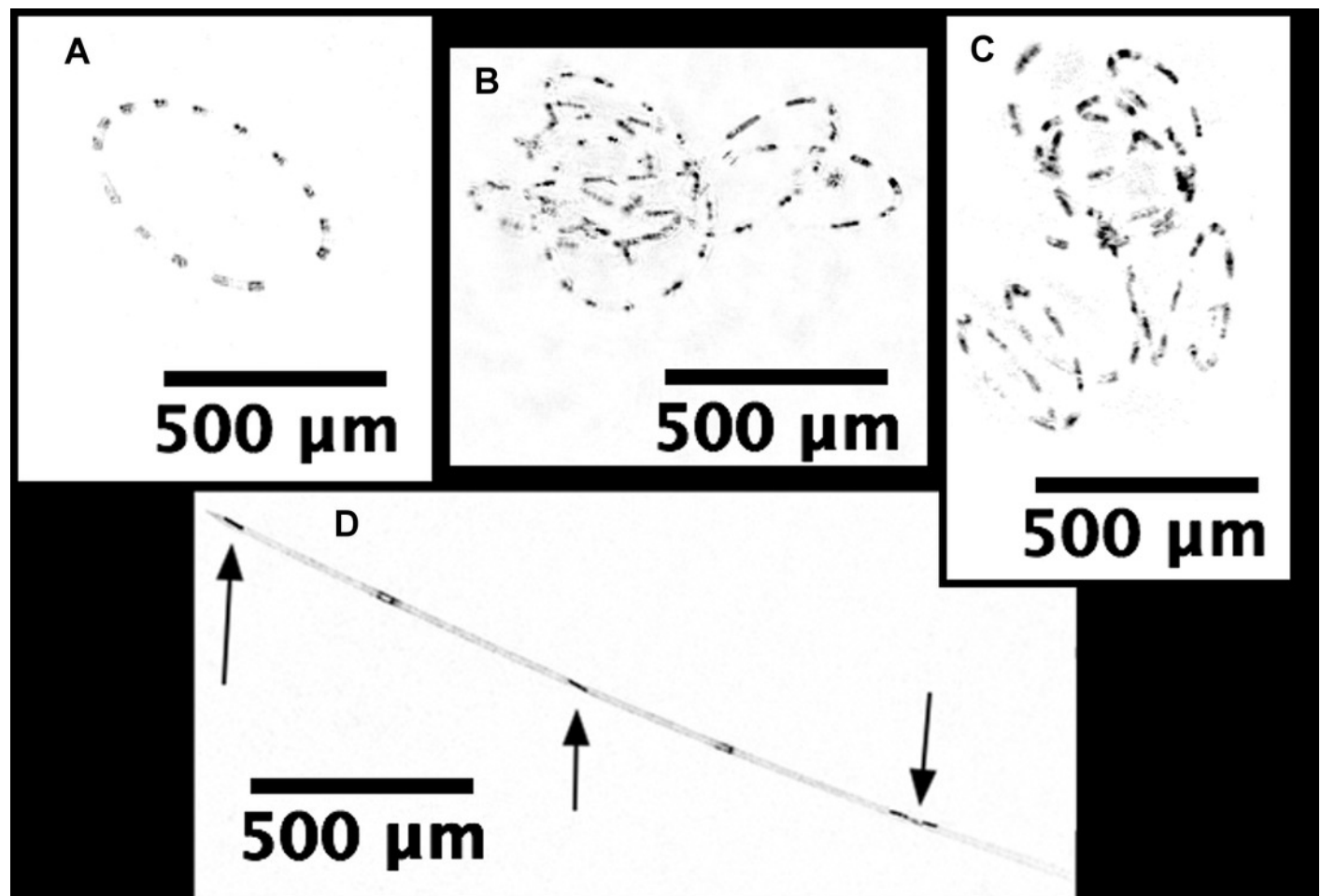
# Figure 7

Time series comparisons between the Aqua MODIS chl *a* data and the *in situ* data collected by the *Honey Badger*'s sensors.

(A) 8-day composite data from Aqua MODIS showing surface chl *a* concentrations (mg m$^{-3}$) near *Honey Badger*'s location. (B) *Hemiaulus* abundance (cells L$^{-1}$). (C) *Rhizosolenia* abundance (cells L$^{-1}$). (D) Biovolume from 11-58 μm bins. (E) Average $F_v$:$F_m$ between 0800-1359 UTC (dark-adapted value). Blue and yellow shaded area indicate the *Hemiaulus* and *Rhizosolenia* bloom. respectively.
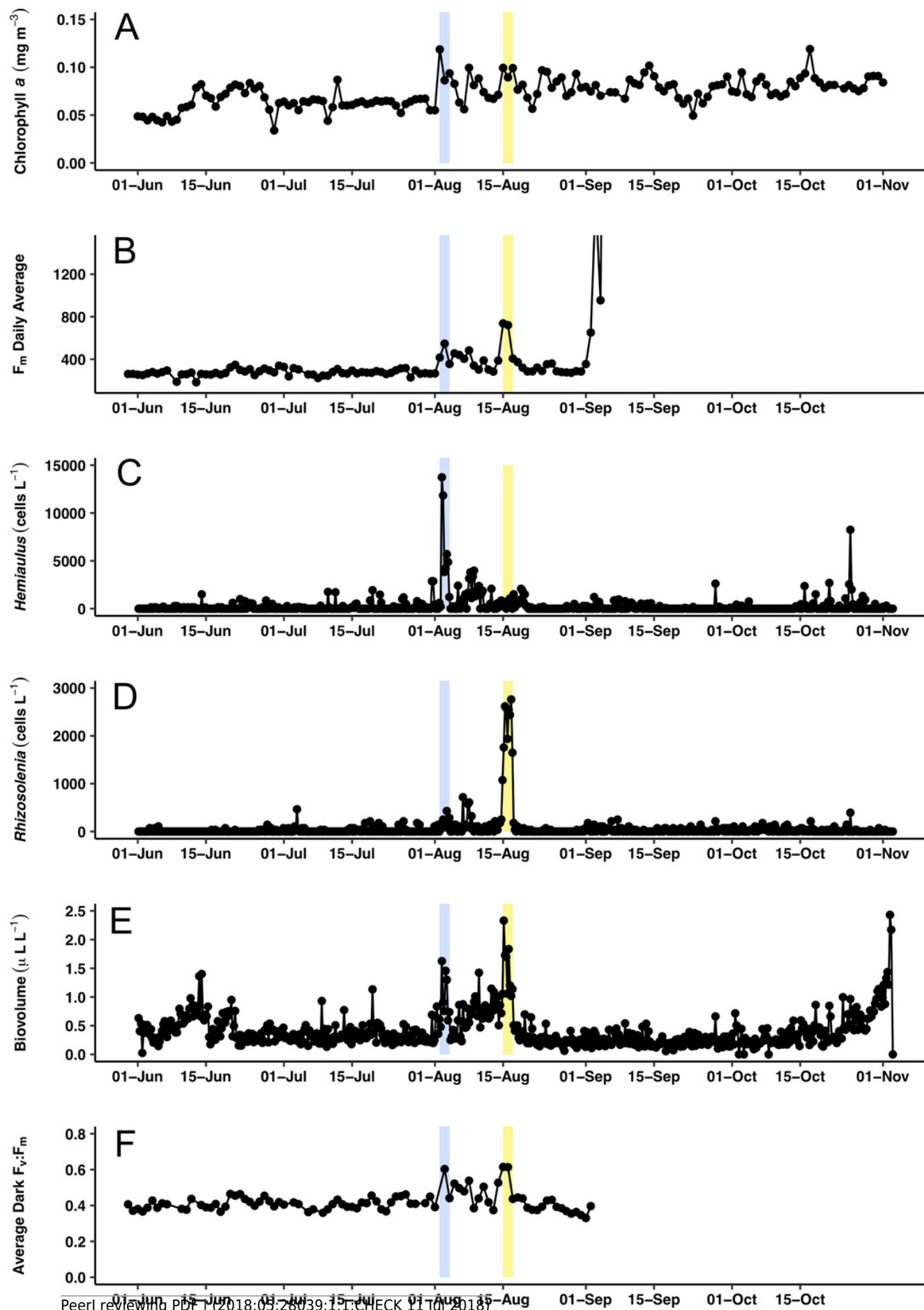
# Figure 8

*Hemiaulus* aggregated and free-living form distribution.

(A-B) Aqua MODIS chl surface concentration and *Honey Badger*'s position. Black dot= mission track position, red-white-black crosshair = *Honey Badger*'s position on day of satellite image. (A) 3 August 2015; *Hemiaulus* bloom B) 16 August 2015; *Rhizosolenia* bloom. (C) Time-series plot of *Hemiaulus* abundance in the free-living or aggregated form. (D) Locations of non-aggregated *Hemiaulus* cells and locations of aggregates. Red triangle = aggregate. Circles = non-aggregated *Hemiaulus* cells L$^{-1}$), size is proportional to abundance. The green area indicates where *Honey Badger* sampled during the SEP time window (15 July– 15 August).
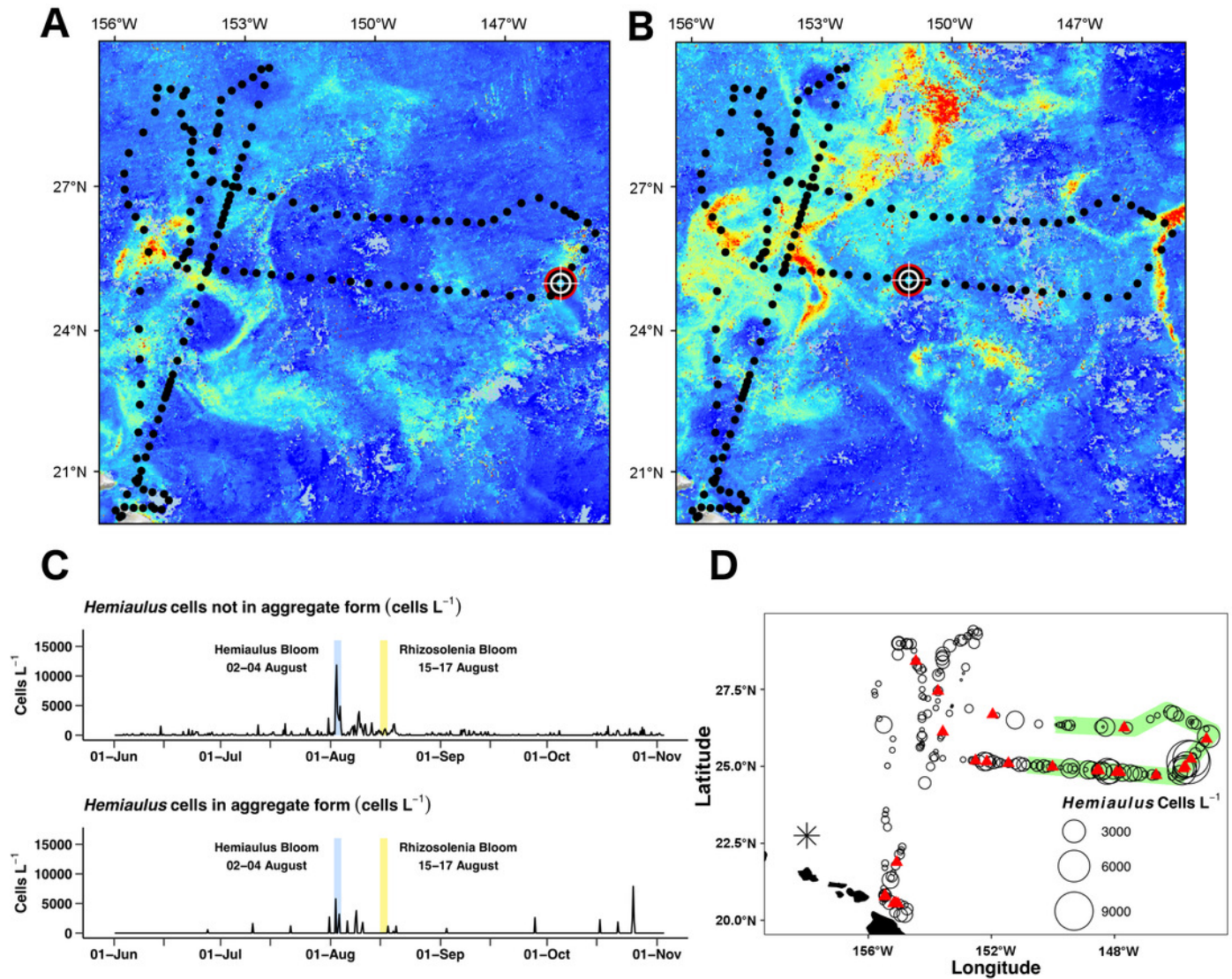
# Figure 9

PhytoFlash $F_v$:$F_m$ diel rhythm sample and iron limitation index.

(A) Sample of the typical diel rhythm observed in the PhytoFlash $F_v$:$F_m$ measurements. The signal is down-regulated during the daytime and returns to the maximum value during the dark period while macro-nutrient limited. Dark bars = 08:00-13:59 UTC (nocturnal period used in the calculation). Light bars = 18:00-02:59 UTC (diurnal period used in the calculation). (B) Time-series of the dark-averaged $F_v$:$F_m$ minus the light-averaged $F_v$:$F_m$. Red points indicate where the sample number did not meet the threshold for calculation (see Methods). Asterisks are points where the data was compromised (see text).
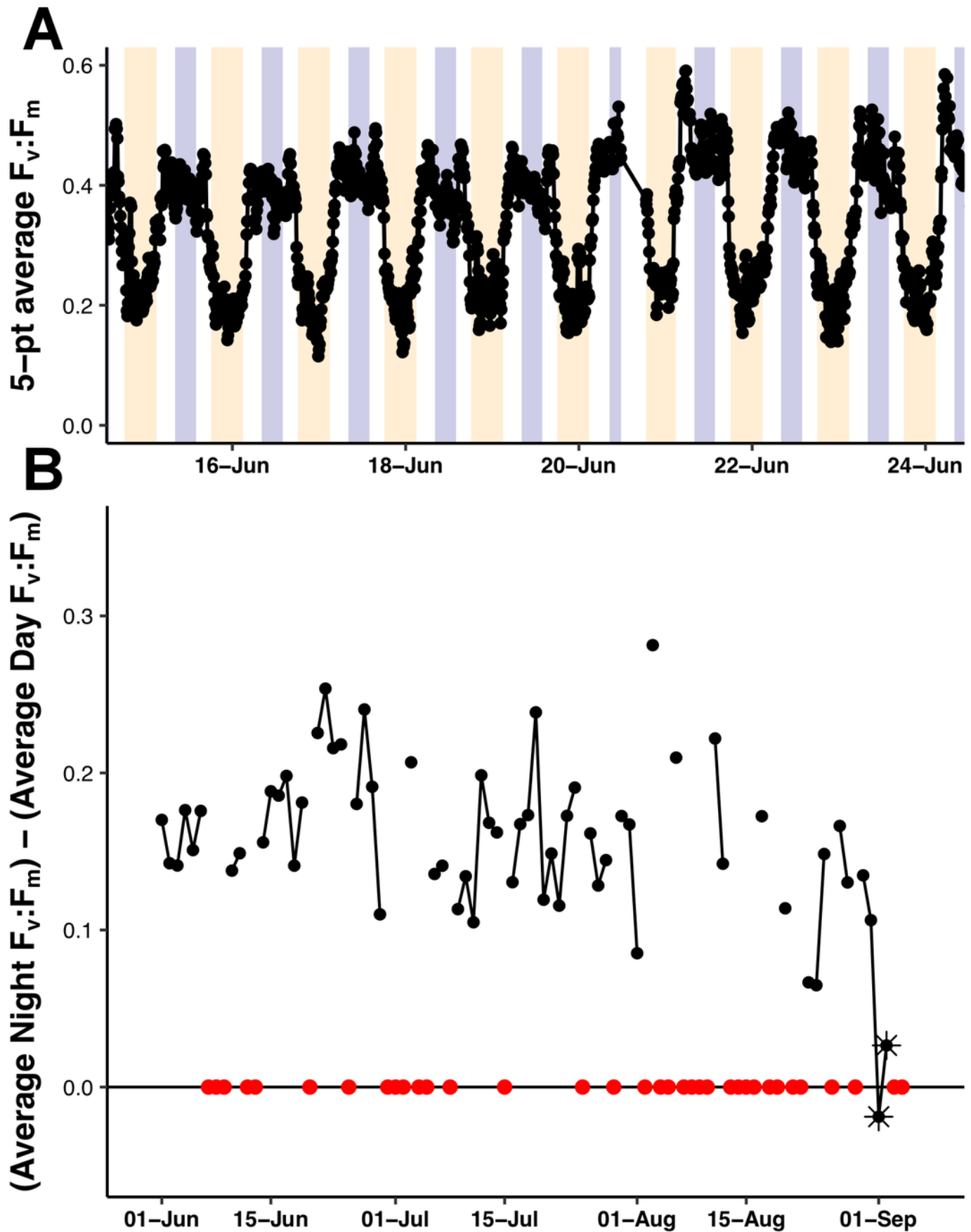
List of the instruments onboard the *Honey Badger*with their locations on the Wave Glider (Fig. 2) and their programmed sample frequency.

| Sensor (location) | Variables (units) | Interval | Available in Near Real Time? |
|---|---|---|---|
| Sea-Bird Scientific's gpCTD (2) | Water Temperature (°C), Salinity, Density (dBar) | 48 hr$^{-1}$ | Yes |
| Turner Designs' C3™ Submersible Fluorometer with Antifouling Coating (2) | Colored Dissolved Organic Mater (CDOM) (RFU), Chlorophyll-a (RFU), and Phycoerythrin Fluorescence (RFU) | 6 hr$^{-1}$ | Yes |
| Turner Designs' C3™ Submersible Fluorometer without Antifouling Coating (2) | Colored Dissolved Organic Mater (CDOM) (RFU), Chlorophyll-a (RFU), and Phycoerythrin Fluorescence (RFU) | 6 hr$^{-1}$ | Yes |
| AirMar Technology's WX Series Ultrasonic WeatherStation® (1) | Air Temperature (°C), Pressure (mBar), Average Wind Speed (knots) and Direction (degrees true) | 6 hr$^{-1}$ | Yes |
| Datawell BV's MOSE (2) | Significant wave height (m) and Direction (degrees true) | 2 hr$^{-1}$ | Yes |
| Cannon G10 Camera (2) | Downward facing camera for imaging the sub-body | 6 hr$^{-1}$ | No |
| Turner Designs' PhytoFlash (4) | $F_o$, $F_m$, $F_v$, Yield ($F_v$:$F_m$) | 6 hr$^{-1}$ | Yes |
| Sequoia Scientific LISST-Holo (5) | Holographic microscopic images of the water | 1 burst of 15 images every 6 hr | No |

*Hemiaulus* aggregate locations and contribution to total *Hemiaulus* abundance.

The *Hemiaulus* aggregate events outside (left) and within (right) the 15 July – 15 August summer export pulse. N = number of aggregates in each 15 image burst at that location. The *Hemiaulus* bloom event is in bold, italicized text.

| Aggregate events outside the SEP | | | | Aggregate Events within the SEP | | | | |
|---|---|---|---|---|---|---|---|---|
| Date (UTC) | n | Location | | *% Hemiaulus* in Aggregates (Total cells L⁻¹) | Date (UTC) | n | Location | | *% Hemiaulus* in Aggregates (Total cells L⁻¹) |
| | | °N | °N | | | | °N | °W | |
| 6/27/15 8:07 | 1 | 28.41 | 154.45 | 66.6 (861) | 7/20/15 17:14 | 1 | 26.25 | 147.68 | 82.9 (1471) |
| 7/10/15 1:06 | 1 | 26.69 | 151.96 | 91.8 (1757) | 7/31/15 15:31 | 1 | 25.80 | 145.01 | 95.0 (2869) |
| 8/17/15 4:01 | 1 | 25.10 | 151.45 | 78.6 (1506) | *8/02/15 10:09* | *3* | *25.24* | *145.52* | *42.0 (13737)* |
| 8/18/15 16:37 | 1 | 25.15 | 152.15 | 15.5 (2080) | *8/03/15 4:29* | *1* | *25.00* | *145.71* | *29.7 (4232)* |
| 8/19/15 10:55 | 1 | 25.18 | 152.51 | 78.6 (1506) | *8/03/15 10:38* | *3* | *24.93* | *145.76* | *56.0 (5702)* |
| 9/2/15 16:29 | 1 | 27.44 | 153.74 | 64.7 (1219) | 8/05/15 17:34 | 2 | 24.71 | 146.65 | 85.1 (2403) |
| 9/27/15 14:14 | 1 | 26.12 | 153.58 | 100.0 (2618) | 8/08/15 0:22 | 1 | 24.81 | 147.83 | 80.7 (3156) |
| 10/15/15 21:22 | 1 | 21.80 | 155.08 | 95.5 (2367) | 8/08/15 6:31 | 2 | 24.81 | 147.93 | 100.0 (3802) |
| 10/20/15 23:22 | 2 | 20.81 | 155.46 | 69.3 (2690) | 8/09/15 19:10 | 1 | 24.86 | 148.50 | 39.0 (2116) |
| 10/21/15 5:28 | 1 | 20.77 | 155.47 | 31.8 (789) | 8/10/15 1:10 | 1 | 24.87 | 148.57 | 75.8 (2367) |
| 10/25/15 0:58 | 2 | 20.54 | 155.18 | 90.1 (2546) | | | | | |
| 10/25/15 7:04 | 1 | 20.56 | 155.11 | 95.7 (8249) | | | | | |
| 10/25/15 13:10 | 1 | 20.54 | 155.04 | 100.0 (2009) | | | | | |